Last glacial fluctuations in the southwestern Massif Central, Aubrac (France): first direct chronology from cosmogenic 10 Be and 26 Al exposure dating

Arthur Ancrenaz, Regis Braucher, Emmanuelle Defive, Alexandre Poiraud, Johannes Steiger

Last glacial fluctuations in the southwestern Massif Central, Aubrac (France): first direct chronology from cosmogenic ^{10}Be and ^{26}Al exposure dating

Arthur Ancrenaz[1]*, Régis Braucher[2], Emmanuelle Defive[1], Alexandre Poiraud[1], Johannes Steiger[1]

[1] Université Clermont Auvergne, CNRS, GEOLAB, F-63000 Clermont-Ferrand, France

[2] Aix-Marseille Université, CNRS-IRD UM34, Collège de France, INRAE, CEREGE BP 80, 13545 Aix-en-Provence Cedex 4, France

*Corresponding author: arthur.ancrenaz@uca.fr

Abstract

The chronology of the late Pleistocene glaciation in the Massif Central, France, is not well documented and there are divergent hypotheses regarding the timing of glacial events in this area. This study aims at reconstructing the chronology of late Pleistocene glacier fluctuations in the Aubrac massif. We present a new set of Be-10 and Al-26 exposure ages from twenty erratic boulders embedded in six glacial landforms. Glacial landforms were sampled to determine the timing of three glacial stades and the deglaciation of the Aubrac Mountains. These new data allowed us to constrain the timing of: (i) the Local Last Glacial Maximum, which is coeval to the early part of Marine Isotopic Stage 2 (MIS 2) (28–24 ka), and (ii) the Grandvals and Bouquincan stades, which are both coeval with the later part of MIS 2 (24–16 ka). Deglaciation occurred during Heinrich Stadial 1 (18–15.6 ka). This new direct glacial chronology is supported by regional paleoenvironmental proxies and it updates the chronostratigraphic framework available for the southwestern Massif Central. Western European atmospheric circulation changes (i.e., a southward shift in North Atlantic storm tracks and Mediterranean influences) during MIS 2 were identified as significant factors controlling glacier growth in the Aubrac Mountains as well as other glaciated mountains within the southwestern Massif Central, such as the Cantal, Margeride and Lozère mountains.

Key words

Late Pleistocene; glacial geochronology; cosmogenic exposure dating; moraine; plateau icefield; Massif Central; Aubrac

1 Introduction

Recent advances in glacial chronology highlight that glaciated areas in Europe did not experience their Local Last Glacial Maximums (LLGMs) synchronously during the late Pleistocene (129-11.7 ka) (Gillespie and Molnar, 1995; Hughes et al., 2013). In the western Alps (Gribenski et al., 2021) and in the eastern Pyrenees (Calvet et al., 2011) for example, the LLGM was probably not coeval with the global Last Glacial Maximum (LGM) between 27.5 and 23.3 ka, *sensu* Hughes and Gibbard (2015). LLGMs in Europe were controlled by both the North Atlantic and Mediterranean atmospheric circulation patterns, which evolve during the late Pleistocene (Domínguez-Villar et al., 2013; Delmas, 2015; Hughes and Woodward, 2017; Monegato et al., 2017; Gribenski et al., 2021; Reixach et al., 2021). This evolution is controlled by the southward displacement of the Polar Jet Front that induced reorganization of atmospheric circulations (Florineth and Schlüchter, 2000; Kuhlemann et al., 2008; Luetscher et al., 2015). In the Massif Central, France, the timing of LLGMs differed from one area to another, according to available relative and indirect chronologies, and thus it provides a key area to identify changes in atmospheric circulation patterns.

Veyret (1978) first proposed a regional and comprehensive synthesis of late Pleistocene glacier fluctuations in the Massif Central based on geomorphological criteria, comprising delimitation of glacier extensions, the prominence of glacial features, the degree of the alteration of moraines and morphostratigraphy. The author thus identified three glaciated areas (Fig. 1), each controlled by topographic and climatic influences. The western glacier group is composed of the Cantal, Monts Dore and Cézallier coalescent glacier systems (Fig. 1). Its LLGM was in MIS 2 based on the limited weathering of glacial deposits (Goër de Hervé, 1972; Veyret, 1978). A large glacier advance following the LLGM, locally named the Recurrence Event (Veyret, 1978), deposited end moraines within the main valleys of the Massif Central, followed by a phase of cirque glaciation that is only represented within the Cantal (Valadas, 1984). The timing of full deglaciation is not well known, but it is associated with

the Last Glacial-to-Interglacial Transition (LGIT) (Veyret, 1978; Valadas, 1984; Vergne, 1991). The southern glacier group was composed of the Margeride and Lozère Mount plateau icefields and by the Velay cirque glacier, that reached its LLGM extent during the MIS 2 (Veyret, 1978). The Aubrac Mountains are located at the margins of the western and southern glacier groups (Fig. 1) (Veyret, 1978). The eastern glacier group corresponds to the small icecap of the Forez. It reached its LLGM extent during the MIS 4 (Etlicher, 1986).

Inferences of climate change from deglacial sequences rely on direct dating tools applied to ice-marginal landforms that provide robust glacial chronology (Kleman and Borgström, 1996; Stokes et al., 2015). In particular, terrestrial cosmogenic nuclides (TCNs) have been widely applied to glacial landforms, such as end moraines, glacial deposits or subglacially eroded bedrock. Resultant exposure ages constrain the timing of the advance and decay of late Pleistocene glaciers (Balco, 2011; Stokes et al., 2015; Allard et al., 2021). Previous reconstruction of the late Pleistocene glaciation of the Massif Central was based on morphostratigraphic evidence and relative correlations with local and regional paleoenvironmental proxies (Goër de Hervé, 1972; Poizat and Rousset, 1975; Veyret, 1978; Valadas, 1984; Etlicher, 1986; Ancrenaz et al., 2020). Indirect paleoenvironmental proxies, such as pollen sequences (Etlicher et al., 1987; Reille and Beaulieu, 1988; Ponel and Russell Coope, 1990; Vergne, 1991; Gandouin et al., 2016; Ponel et al., 2016) or sedimentological stratigraphies (Valadas, 1984; Laville et al., 1986; Van Vliet-Lanoë et al., 1991), are available and provide indirect chronological boundaries for glacier fluctuations. However, resulting chronologies differ for the various glaciated areas of the Massif Central (cf. Etlicher and Goër de Hervé, 1988; Defive et al., 2019). Hence, without direct dating of glacial deposits, important uncertainties and inconsistencies remain, especially concerning the timing of both the LLGM and full deglaciation. During the last glacial cycle, two periods, locally named the Early and Late Pleniglacial (*sensu* Laville et al., 1986; Van Vliet-Lanoë et al., 1991), that correlate with Marine Isotopic Stage 4 (MIS 4; 71−57 ka; Lisiecki and Raymo, 2005) and MIS 2 (29−11.7 ka; Lisiecki and Raymo, 2005), respectively, were recognised as two major phases of glacier growth in the Massif Central (Etlicher and Goër de Hervé, 1988; Defive et al., 2019). In general, in the literature and according to the considered glaciated area, the LLGM is attributed to one of these two periods.

The objectives of the present study were to assess the existing relative glacial chronologies (Poizat and Rousset, 1975; Veyret, 1978; De Goër et al., 1994; Ancrenaz et al., 2020) and to provide the first direct dating chronology for fluctuations of the Aubrac plateau icefield. In that respect, key glacial landforms identified by the morphostratigraphy are targeted. In combination with an extensive literature review on glacier fluctuations within the Massif Central, a revised and comprehensive chronostratigraphic framework is proposed that focuses on the southwestern Massif Central. Furthermore, inferences of glacier fluctuations from regional paleoclimates, especially favourable glacier-growth phases, are proposed.

2 Study area

The Aubrac Mountains, in the south western Massif Central, extend over 1300 km^2 and culminate at the Signal de Mailhebiau at 1467 m above sea level (a.s.l.) (Fig.1). Three geomorphological subareas divide the Aubrac Mountains (Fig. 2). The Aubrac Highlands are composed of a SSE to NNW alignment of rounded summits composed of Miocene volcanic rocks (Goër de Hervé et al., 1991; Leibrandt, 2011). This topographic ridge extends along 25 km with an elevation decrease from 1400 m in the SSE to 1200 m in the NNW. The Aubrac Highlands separate the two following subareas: the Aubrac Plateau to the northeast and Aubrac Valleys to the southwest (Fig. 2). The Aubrac Plateau, with elevations between 1000 and 1200 m, formed within granitic Carboniferous rocks (Couturié, 1977). The Bès valley oriented from SSW to NNE represents the major hydrographic basin that drains this subarea. In addition, the Aubrac Valleys, incised into the margins of the highlands, are deep and steep valleys that are 10 to 20 km long and cut in metamorphic rocks.

The Aubrac Mountains constitute the first orogenic obstacle that is encountered by atmospheric low-pressure systems pushed by the westerlies from the North Atlantic into the European continent. Current precipitation is characterised by a maximum during winter and a minimum during summer (Jubertie, 2006). Precipitation of more than 1500 $mm.y^{-1}$ was recorded (1980-2010) for the Aubrac Highlands at Nasbinals, 1284 m a.s.l. (ID station: 48104002; https://donneespubliques.meteofrance.fr). Snowfall and snow cover during winter highlights the role of the Aubrac Highlands as a preferential area for snow accumulation (Valadas and Veyret, 1981).

3 The late Pleistocene Aubrac glaciation

3.1 Evidence for a plateau icefield glaciation

The topographic setting of the Aubrac Mountains exert a strong control on the spatial extension and dynamics of the former plateau icefield. The plateau icefield accumulation zone was centred on the Aubrac Highlands (Fig. 2), with an estimated thickness between 200 and 300 m (Poizat and Rousset, 1975; Ancrenaz et al., 2020). The ice divide of the plateau icefield followed the SSE–NNW orientated Aubrac Highlands and separated two distinct zones of glacial dynamics. The Aubrac Plateau that was situated to the east of the ice divide and was predisposed to the establishment of a plateau glacier because of its relatively low-lying topography (Figs. 2-3). This plateau glacier is recorded by ice-scoured knock and lochan topography, with bedrock forming *roches moutonnées* and rock basins partly infilled by glacial or associated sediments (Poizat, 1973; Veyret, 1978; Goër de Hervé et al., 1994; Ancrenaz et al., 2020). According to the orientation of *roches moutonnées* (Ancrenaz et al., 2020) and the dispersion of erratics (Poizat and Rousset, 1975), the Bès valley was the preferential drainage route for the Aubrac plateau glacier. In the Aubrac Valleys, isolated glacial deposits were associated to phases of glacier retreats and overdeepened morphologies were recognised and associated with subglacial erosion by outlet valley glaciers (Rousset, 1963, 1970; Poizat and Rousset, 1975).

Local plateau icefields are sensitive to climatic changes when the regional Equilibrium Line Altitude (ELA) is close to the plateau elevation. Indeed, climatic changes inducing variations in ELAs lead to substantial changes in the distribution of glacier ablation/accumulation zones, i.e. small increase or decrease of the ELA induce significant glacier advance or retreat in response to strong modification of the accumulation/ablation zones distribution (Manley, 1955; Rea et al., 1999; Rea and Evans, 2003; Boston et al., 2015). This observation is in accordance with the landform assemblage identified in the Aubrac Plateau, indicating rapid and *in situ* glacier downwasting during deglaciation (Section 2.3) driven by small changes in the ELA. The accumulation zone of the Aubrac plateau icefield was located along the topographic ridge of the Aubrac Highlands (Poizat and Rousset, 1975; Ancrenaz et al., 2020). The mass balance adjustment of this zone is argued to control the former glacier extent in the Aubrac Plateau and in Aubrac Valleys (Poizat and Rousset, 1975; Ancrenaz et al., 2020). A glacier advance (or

retreat) in the Aubrac Plateau was coeval with a glacier advance (or retreat) in the Aubrac Valleys in response to the thickening (or thinning) of the glacier accumulation zone in the Aubrac Highlands.

3.2 Deglaciation sequence in the Aubrac Plateau

The majority of glacial landforms in the Aubrac Mountains are located on the Aubrac Plateau (Figs. 2-3). Three distinct glacier advances were reconstructed in previous studies from investigations of landform assemblages (Table 1, Fig. 3). First, the extent of the LLGM was defined by the maximum extent of volcanic erratic boulders on the Aubrac Plateau (Figs. 2, 3A) that matched the maximal extent of glacial sediments (Veyret, 1978; Goër de Hervé et al., 1994). On this basis, the LLGM outer limit matched the occurrence of tors or saprolite associated with periglacial environments (Goër de Hervé et al., 1994; Ancrenaz et al., 2020). Moreover, the Allatieux end moraine (1199 m), which corresponds to a group of three discontinuous ridges that are one hundred metres long, demarcates the LLGM in the Aubrac Plateau (Table 1; Fig. 4A.) (Ancrenaz et al., 2020). This landform matches (i) the maximal extent of erratic boulder dispersion and (ii) the occurrence of periglacial features such as bloc fields or tors. The fresh aspect with no boulder weathering rind and the well preserved glacial sediments support an interpretation of that the LLGM correlates with the global LGM (Veyret, 1978; Ancrenaz et al., 2020).

The end of the LLGM is characterised by a pronounced retreat of the Aubrac plateau icefield (Fig. 3C). An early still-stand is recorded in the Bès valley at the Longevialle end moraine (1040 m a.s.l.), composed of a group of parallel and subdued ridges with pronounced crest attenuation (Table 1; Fig. 4B). It is located only 2 km behind the maximum erratic boulder dispersion that demarcates the LLGM limit and also behind fluvio-glacial sediments deposited during LLGM retreat. Subsequent glacier recession is recorded by numerous, well-preserved glacial, glacio-fluvial and glacio-lacustrine sediment landform assemblages that were identified within the Aubrac Plateau (Poizat, 1973; Poizat and Rousset, 1975; Veyret, 1978; Goër de Hervé et al., 1994; Ancrenaz et al., 2020). These sediments were associated with the formation of ice-dammed lakes which infilled the major depressions of the plateau and comprise kame hills and proglacial outwash. These landforms suggest *in situ* glacier downwasting (Livingstone et al., 2010; Lovell et al., 2019). Indirect chronological control on this phase of deglaciation was obtained from ^{14}C dating of sediment sequences infilling depressions along deglaciated areas of the

Aubrac Mountains. At the Roustières site, located in the Aubrac Plateau inside the LLGM limit (see Fig. 2 for the location), proglacial lake sediments are dated to the Oldest Dryas between 17.7 and 16.6 ka (Gandouin et al., 2016; Ponel et al., 2016). However, the base of the sequence was not reached and thus these ages provide only a minimum age constraint.

A glacier re-advance interrupted this retreat sequence and truncating these sediments and landforms and depositing till. This glacial event is referred to as Grandvals Stade (Fig. 3C) (Poizat, 1973; Veyret, 1978; Ancrenaz et al., 2020). It is demarcated in the Bès valley by the Grandvals end moraine (1059 m a.s.l.) (Table 1; Fig. 5A). This landform is divided into two features: one on each valley flank. Fluvioglacial deposits associated with the Grandvals end moraine formed proglacial outwash that aggraded overLLGM deposits. After the glacier retreats, the Bès River deeply incised the Grandvals end moraine and constructed fluvial terraces (Ancrenaz et al., 2020). Other end moraines in the Aubrac Plateau encompassed truncated LLGM deposits and were correlated to the Grandvals stade (Ancrenaz et al., 2020). These include the Rateylou end moraine. It is located in a flat depression between the Bès and the Rimeize catchments (Table 1; Fig. 5B). This landform is composed of two subdued ridges and is correlated with the Grandvals stade.

A final glacier advance in the Bès valley is recorded by the Bouquincan end moraine that is located up-valley from the Grandvals end moraine (Table 1; Fig. 3B) (Ancrenaz et al., 2020). This end moraine contains fluvio-glacial sediments deformed by glacio-tectonic processes, interpreted as the result of a glacier advance in the Bès valley. All glacial deposits that were identified in the Aubrac Highlands were associated with the final plateau icefield decay. For example, the Bonnecombe till demarcated the very last deglaciation phase as it is located at the Bonnecombe pass (1340 m a.s.l.), one of the most elevated area of the Aubrac Mountains.

The Aubrac plateau icefield was a climatically-sensitive system located between the western and southern sectors of the Massif Central. Three distinct groups of end moraines record three glacier advances in the region, especially along the Bès valley (see section 3.2), but the absolute ages of these moraines (and thus the associated advances) is poorly constrained. This paper addresses this through

TCN dating of end moraines and erratic boulders and in doing so establishes, for the first time, a direct chronological framework for the late Pleistocene glacial history of the Aubrac Mountains.

4 Be-10 and Al-26 exposure dating

4.1 Sampling strategy, collection and preparation

This study aims to determine the timing of three main glacier advances, as well as the timing of deglaciation in the Aubrac Mountains (section 3.2). Glacial landforms and deposits in the identified from the literature were checked in the field and candidates for TCN dating selected according to two requirements. First, glacial landforms should be clearly identified by morphostratigraphic evidence In that respect, end moraines were especially targeted (Kleman and Borgström, 1996). Secondly, the glacial landform or deposit should match prerequisites for sampling, especially the availability of moraine boulders and low post-depositional disturbance from natural processes or anthropogenic activities (Figs. 4, 5, and 6).

Sample collection was guided by recommendations established elsewhere (Putkonen and Swanson, 2003; Dunai, 2010; Heyman et al., 2016). The availability of dateable moraine boulders limited the number of samples per landform. For subdued end moraines, three samples were collected when available (Putkonen and Swanson, 2003). Tall boulders with their bases broadly embedded in the landform were targeted (Heyman et al., 2016). Rock samples with a thickness of between one and three centimetres were obtained from top and flat surfaces of moraine boulders, using a hammer and a chisel.

Samples were prepared for the extraction of Be-10 and Al-26 (Brown et al., 1991; Merchel and Herpers, 1999). Rock samples were crushed and sieved. A grain size between 0.25 and 1 mm was chosen for further analysis. After magnetic separation using a Frantz Barrier separator, the nonmagnetic grains (including quartz) were subjected to leaching with H_2SiF_6 and HCl to eliminate non-quartz minerals. Three partial dissolutions were performed with HF to eliminate atmospheric ^{10}Be. According to Merchel et al. (2008), ~0.15 g of a homemade (3025±9 ppm) ^{9}Be solution was then added to the solution to fix the $^{10}Be/^{9}Be$ ratio. To determine if an ^{27}Al spike is needed, natural concentrations of ^{27}Al were measured in liquid aliquots by inductively coupled plasma–optical emission spectrometry (ICP–OES, Thermo Icap6500). Quartz was totally dissolved in 40% HF solution. Afterwards, beryllium and aluminium were

extracted by successive anion and cation resins. Finally, the hydroxides $Be(OH)_2$ and $Al(OH)_3$ were heated at 800°C for one hour. The resulting powders were mixed with niobium (BeO) or silver (Al_2O_3).

All ^{10}Be and ^{26}Al measurements were performed at the French Acceleratory Mass Spectrometry (AMS) National Facility "ASTER" located at CEREGE in Aix-en-Provence, France (Arnold et al., 2010). Be-10 and Al-26 were determined for all samples except for AU31, AU32 and AU33 for which only Be-10 measurements are available. Be-10 data were adjusted to the ASTER in-house standard, "STD11", with a Be-10/Be-9 ratio of $(1.191\pm0.013)x10^{-11}$ (Braucher et al., 2015) and the Be-10 half-life of $(1.387\pm0.0012)x10^{6}$ years (Chmeleff et al., 2010; Korschinek et al., 2010). Al-26/Al-27 ratios were calibrated with an ASTER in-house standard, "SM-AL-11", with a ratio of $7.401\pm0.064x10^{-12}$ (Merchel and Bremser, 2004) assuming an Al-26 half-life of $7.05\pm0.17x10^{5}$ years (Samworth et al., 1972).

The parameters above imply an Al-26/Be-10 spallation production ratio of ~6.61±0.52. Reported analytical uncertainties include counting statistics, machine stability (~0.5% for ^{10}Be; Arnold et al., 2010), and blank correction. The Be-10/Be-9 and Al-26/Al-27 blank ratios were $2.45x10^{-15}$ (± 29%) and $9.00x10^{-16}$ (± 100%), for AU01 to AU17 samples respectively. The Be-10/Be-9 blank ratio was $2.60x10^{-15}$ (± 15%) for theAU31, AU32 and AU33 samples.

4.2 Minimum Exposure Age (MEA) calculation

Be-10 and Al-26 exposure ages were calculated using the CHRONUS-Earth online calculator v.3 (Balco et al., 2008) (http://stoneage.ice-d.org/math/v3/v3_age_in.html). Cosmogenic Be-10 and Al-26 production rates at Sea Level and High Latitudes (SLHL) from spallation were computed from default calibration datasets from Borchers et al. (2016), with: 4.132 ± 0.218 at.g^{-1}.y^{-1} for Be-10 and 29.950 ± 2.955 at.g^{-1}.y^{-1} for Al-26. Production rates at SLHL are scaled using the Lal-Stone time corrected scaling scheme (Lal et al., 1991; Stone, 2000), the ERA40 atmosphere model and the magnetic field reconstruction from Lifton (2016). Corrections for topographic shielding were applied following Dunai (2010) and using the inclination of the visible horizon from each sample point extracted from a Digital Elevation Model (DEM) in GIS software (ArcGis 10.3v) and compiled in Table 2. The rock density was set to 2.65 g.cm^{-2} for all samples (Table 2). Contribution from muons were calibrated according to Balco (2017).

Calculated exposure ages for a given nuclide concentration is named the Minimum Exposure Age (MEA) because: (i) no correction for post-glacial denudation nor for snow cover were applied, and (ii) simple exposure histories, without pre-exposure to cosmic rays, were assumed (see section 5.2 for more details). Hereafter, MEAs were expressed with their external uncertainty that includes analytical uncertainty and production rate uncertainty. In order to compare Be-10 and Al-26 MEAs obtain from a glacial landform, for MEA groups with n ≤ 3, the reduced chi square statistic (X_R^2) was used. Only Be-10 MEAs were compared for the Bonnecombe site. For a MEA group with a $X_R^2 \leq 1$, an uncertainty-weighted mean was calculated with the standard deviation of the uncertainty-weighted mean. For MEA groups with a $X_R^2 > 1$, the sample with the farthest MEA from the uncertainty-weighted mean was manually rejected and interpreted as an outlier. Outliers are repeatedly rejected until we obtained a $X_R^2 \leq 1$ or we obtained a MEA group with n < 3 for which no uncertainty-weighted mean was calculated. Manually rejected MEAs were interpreted as the effect of geomorphologic processes and are discussed in section 5.2 below.

5 Results and interpretations

5.1 Minimum Exposure Ages

Twenty moraine boulders were sampled from six different glacial landforms. Resultant cosmogenic nuclide measurements and MEAs, with their external uncertainty, were compiled in Tables 2 and 3. Two boulders (AU16 and AU17) were taken from the Allatieux end moraine crests (Figs. 4A and 6). A clustered group of MEAs is obtained, between 25.41±2.14 to 21.34±3.11 ka, with an uncertainty-weighted mean of 24.29±1.28 ka. Three samples (AU10, AU11 and AU13) were collected from boulders embedded in the Longevialle end moraine flattened crests (Figs. 4 and 5B). MEAs range from 18.12±2.72 to 53.86±4.72 ka and provided the most scattered results in our dataset. No uncertainty-weighted mean was calculated. Three samples were taken from the crest of the Grandvals end moraine (AU13, AU14 and AU15) at the western end of the landform (Figs. 5A and 6). MEAs were clustered, between 21.55±2.05 to 12.19±1.57 ka, with an uncertainty-weighted mean of 20.43±0.93 ka (Table 3). Only the Al-26 MEA from the AU14 sample was interpreted as an outlier. Four moraine boulders embedded in two features composing the Rateylou end moraine (AU03, AU04, AU05 and AU06) gave

scattered MEAs from 2.17±0.41 to 20.55±1.84 ka (Table 3; Figs. 5B and 6). No uncertainty-weighted mean was calculated. In addition, two isolated erratic boulders at the Rateylou site (AU01 and AU02) were sampled near the end moraine (Fig. 5B) and MEAs ranged from 6.55±0.65 to 21.48±1.86 ka. At the Bouquincan end moraine, three samples (AU07, AU08 and AU09) were taken from boulders with low heights: < 0.5 m above the ground (Fig. 3B). Results ranged from 6.84±1.41 to 18.27±1.66 ka. An uncertainty-weighted mean of 16.59±0.9 ka was calculated with rejection of the AU09 sample. Finally, samples AU31, AU32 and AU33 are collected from moraine boulders embedded in the Bonnecombe glacial deposit (Figs. 5C and 6). Only ^{10}Be MEAs are available, and calculated MEAs are 18.66±1.60 (AU31), 16.60±1.43 (AU32) and 16.68±1.48 ka (AU33), with a calculated ^{10}Be uncertainty-weighted mean of 16.64±1.03 ka.

5.2 Glacial landform age

The distribution of exposure ages on end moraines often displays scattered results for the same landform (Heyman et al., 2011; Applegate et al., 2012). Two common explanations are identified (see Heyman et al., 2011): incomplete exposure and the pre-exposure. Boulders with incomplete exposure tend to underestimate ages for end moraine formation. This generally reflects post-depositional processes, such as erosion (e.g. moraine matrix erosion), leading to the landform lowering and smoothing and to boulder exhumation. Exhumed boulders by post-depositional processes, were exposed during a shorter period than the true landform age (Zreda et al., 1994; Putkonen and Swanson, 2003; Putkonen and O'Neal, 2006; Chevalier et al., 2011; Heyman et al., 2011; Palacios et al., 2019; Allard et al., 2020). Then, boulder with incomplete exposure the end moraine depositionThis is the case for outliers with younger MEAs than the uncertainty-weighted mean: AU09 (Table 3; Fig. 7). AU01, AU03 and AU04, from the two Rateylou sites, provided Holocene MEAs (11.7 ka to present) that were younger than expected and interpreted as moraine boulders with incomplete exposure histories (Table 3; Fig. 7). The proximity with quarries (> 100 m; Fig. 5C) could lead to potential modifications of the glacial landform morphology, especially exhumation of buried boulders. For the AU14 moraine boulder, only the Al-26 MEA was interpreted as an outlier since the Be-10 measurement is coherent for the landform age (Table 3; Fig. 7).

Conversely, moraine boulders with pre-exposure provide overestimated ages for moraine deposition due to inherited cosmogenic nuclides from a previous episode(s) of exposure (Heyman et al., 2011). Pre-exposed boulders were estimated to account to 3% of exposure ages from datasets analysed in Putkonen and Swanson (2003). In our dataset, only one moraine boulder with a much older MEA than others was identified: AU11 (Table 3; Fig. 7). As this moraine boulder was associated with a glacial landform inside the LLGM extent, it was interpreted as an overestimated MEA due to cosmogenic nuclide inheritance.

Geomorphological context provides a strong control on processes affecting moraine boulder exposure history and MEA scattering (Palacios et al., 2019; Tompkins et al., 2021). In the Aubrac Mountains, post-depositional erosion of end moraines is argued to be low because: (i) subdued ridges were poorly affected by post-depositional processes such as run-off or slope destabilization (Putkonen and Swanson, 2003) and (ii) the sedimentological composition of these glacial landforms, dominated by sand, gravel and boulders (Veyret, 1978; Ancrenaz et al., 2020), favoured end moraine stabilization (Tompkins et al., 2021). These local geomorphological settings were concordant with a rapid stabilization of glacial landforms after their deposition. As a consequence, a MEA cluster and its uncertainty-weighted mean is argued to best represent the age of the moraine stabilisation (Allard et al., 2020; Tomkins et al., 2021). The age of the end moraine deposition is best represented by the oldest exposure age obtained on the glacial landform (Zreda et al., 1994; Putkonen and Swanson, 2003; Briner et al., 2005; Chevalier et al., 2011; Heyman et al., 2011; Chevalier and Replumaz, 2019). Considering this interpretation, glacial landform stabilization (best approximated by the corresponding uncertainty-weighted mean) occurred rapidly after the landform deposition (best approximated by the corresponding oldest MEA) in the Aubrac Mountains (Table 3; Fig. 7).

5.3 Three distinct glacial stades in the Aubrac Mountains

The LLGM is dated at the Allatieux end moraine to 25.41 ± 2.14 ka (Table 3). The Aubrac plateau icefield covered approximately 500 km^2, with outlet valley glaciers in the Aubrac Valleys of 6 to 10 km in length (Figs. 2 and 8) and an ELA estimated at 1331 ± 10 m a.s.l. (Ancrenaz et al., 2020). Eastward, glacier margins terminate against topographic constraints (i.e., reverse slopes), which restricted plateau icefield extension (Figs. 2, 3A and 8). After the LLGM, the Aubrac plateau icefield retreated first back

onto the plateau. A first glacial stillstand is documented by the Longevialle end moraine dated to 24.31±2.7 ka (Table 3). According to stratigraphic observations, the extension of glacier-free areas related to this glacier retreat can be estimated (Poizat and Rousset, 1975; Veyret, 1978; Ancrenaz et al., 2020), and the deglaciated area after the LLGM is at least half that of the LLGM area (Figs. 8-9). The Grandvals stade is dated at three sites: the Grandvals end moraine (21.55±2.05 ka), the Rateylou end moraine (20.55±1.84) and the Rateylou isolated erratics (21.48±1.86 ka) (Tables 1 and 3, Figs. 7-9). These ages overlap, suggesting that these landforms are probably related to the same glacier advance (Kirkbride and Winkler, 2012; Blomdin et al., 2016), as suggested by the morphostratigraphic framework established for the Aubrac Mountains (Section 2.3). The last glacial stade is documented by the Bouquincan end moraine and dated to 18.27±1.66 ka. During this stade, the plateau icefield was restricted to the Aubrac Highlands with outlet glaciers confined to the main head valleys (Fig. 8). Steps of the following glacier retreat are not recognised in the field. Subsequent stillstands during glacier retreat were not recognized but tills were identified over the Aubrac Highlands (Goër de Hervé et al., 1994). The Bonnecombe till is one of these deposits associated with the Aubrac plateau icefield decay (Table 1; Fig. 8). The ages of both the Bouquincan stade and the Bonnecombe till (18.66±1.60 ka) suggest a rapid deglaciation. This trend is supported by paleoenvironmental reconstruction from the Roustières site (see Figs. 2 and 8) (Gandouin et al., 2016; Ponel et al., 2016), where periglacial conditions in the Aubrac Plateau were active between 17.7 and 16.6 ka, with persistent winter snow cover in the Aubrac Highlands.

6 Chronological update of the southwestern Massif Central chronostratigraphy: correlations and climatic inferences

The direct glacial chronology presented in this work is in good agreement with the existing morphostratigraphic framework established in the Aubrac Mountains (Section 2.3) and provides robust chronological control of past fluctuations of the Aubrac plateau icefield. Considering that the Aubrac plateau icefield is a valuable climatic proxy (Section 2.2), this new chronology highlights the main climatic conditions for the southwestern Massif Central and allows us to update and revise the regional chronostratigraphy.

6.1.1 The GS-3: establishment of full glacial conditions

In the western Massif Central, a successive and gradual climatic deterioration with increasingly colder temperatures started with the onset of MIS 2 (Laville et al., 1986) at ~29 ka (Lisiecki and Raymo, 2005). A cold culminationis recorded and primarily associated to the beginning of the MIS 2 (Laville et al., 1986), and then correlated to approximately 25 ka (Van Vliet-Lanoë et al., 1991). Dating of the infilling of thermal contraction cracks in discontinuous permafrost in the Aquitaine basin resulted in ages between 27 and 25.5 ka BP and suggests a climatic downturn at the beginning of MIS 2 (Bertran et al., 2014). This event is synchronous with the LLGM in the Aubrac Mountains, dated to 25.41±2.14 ka. This is also coeval with the global LGM between 27.5 and 23.3 ka, *sensu* Hughes and Gibbard (2015), Greenland Glacial Stadial 3 (GS-3) between 27.5 and 23.3 ka (Rasmussen et al., 2014), Heinrich Stadial 2 (HS2) between 26.5 and 24.3 ka (Sanchez Goñi and Harrison, 2010) and finally the $\delta^{18}O$ minimum of the 7H record from the Sieben Hengste cave (northern Alps) centred on 25.3 ka (Luetscher et al., 2015). Moisture advection from the Mediterranean Sea, enhanced by cyclogenesis, led to favourable conditions for glacier growth in the circum-Mediterranean mountains (Florineth and Schlüchter, 2000; Kuhlemann et al., 2008; Luetscher et al., 2015; Monegato et al., 2017), such as the Pyrenees (Delmas et al., 2011; Reixach et al., 2021), the Alps (Monegato et al., 2017; Wirsig et al., 2016) and the Iberian Peninsula (Domínguez-Villar et al., 2013).These cold and wet climatic conditions related to enhanced Mediterranean influences probably triggered the LLGM in the Aubrac Mountains, as well a simultaneous LLGM in other glaciated mountains of the southwestern Massif Central (Cantal, Margeride and Lozère Mountain). In this area, gelifluction and gelifraction deposits on non-glaciated slopes should be correlated to this period (Fig. 9) because effective gelifluxion or gelifraction processes are supported by cold and wet climatic conditions (Valadas, 1984) that reached their optimum during this period The question of an asynchronous LLGM between the southwestern (Aubrac, Cantal, Margeride and Lozère Mountain) and the eastern Massif Central remains.

6.1.2 The GS-2.1: aridity, a limiting factor for glacier growth

After the global LGM, full glacial conditions characterised by a cold and arid climate (Laville et al., 1986; Reille and Beaulieu, 1988; Van Vliet-Lanoë et al., 1991) prevailed across the whole Massif Central

during GS-2.1 (22.9 to 14.7 ka; Rasmussen et al., 2014). For example, at the Haute-Laugerie site (44°57′11″ N; 1°00′12″E), reconstructed anomalies for mean annual precipitation are -800 mmy^{-1} and -7.4 to -4.7 °C for mean air temperatures at ~21 ka (Lécuyer et al., 2021). These data are comparable to those reconstructed from the Lake Bouchet sequence (see Fig. 1 for location), with -6 °C for the annual temperature anomaly and -772 mm for the annual precipitation anomaly (Peyron et al. 1998). Between ~24 to 17 ka, the Aubrac plateau icefield was in recession reflectingcold and dry climatic conditions in the Massif Central. It is suggested here that the aridity recorded in the Aquitaine Basin and in the Massif Central was the limiting factor for glacier growth during this period. In the Alps, the progressive starvation of Mediterranean moisture triggered glacier recession (Luestcher et al., 2015; Wirsig et al., 2016 and references therein). On non-glaciated slopes of the southwestern Massif Central, reduced gelifluction and gelifraction processes were associated with this period and highlight the climatic aridity (Valadas, 1984; Van Vliet-Lanoë et al., 1991; Degeai and Pastre, 2009) (Fig. 9). However, two glacier advances at this time, the Grandvals stade (21.55±2.05 ka) and the Bouquincan stade (18.27±1.84 ka), indicated two phases of glacier favourable climatic conditions. Important glacier advances in the Alpine foreland at 21–20 ka were reported (Wirsig et al., 2016 and references therein). For example, the Tagliamento lobe (Italy) advanced at 23–21 ka (Monegato et al., 2007) and the Durance glacier (France) advanced at approximately 20 ka (Jorda et al., 2000). The Eurasian ice sheet reached its maximal extent at ~21 ka (Hughes et al., 2015).

This period is also characterised by climatic instabilities recorded in the western Massif Central as indicated by archaeological stratigraphic investigations (Laville et al., 1986). In the eastern Massif Central (Velay Mountains), slope instability (dated to ~20 ka) is interpreted as possible permafrost disappearance (Poiraud, 2012). This period is also coeval with the deposition of aeolian coversands in the Aquitaine Basin, dated to 24 - 14 ka, in association with cold and dry climatic conditions (Sitzia et al., 2015). During this phase, periods of reduced coversand accumulation, linked to reduced aeolian activity, permafrost degradation and/or milder climatic conditions, were reported between 20.8 and 17.0 ka (Sitzia et al., 2015). The HS1 started with the progressive cooling of the North Atlantic between 19 and 17.4 ka (Pascual et al., 2020). Effects of this cooling in the southwestern European climate were

reported between 18 to 15.6 ka (Sanchez Goñi and Harrison, 2010) and were characterized by cold and arid conditions (Kageyama et al., 2005; Ludwig et al., 2018). These conditions were associated with discontinuous permafrost in the Aquitaine basin (Lenoble et al., 2012) and cold and dry climates in the Massif Central despite longer and warmer summers (Reille and Beaulieu, 1988). The Grandvals and Bouquincan stades were potentially triggered by short-lived or slight climatic changes during the GS-2.1, especially a wetter period in overall dry climatic conditions. At the scale of the entire Massif Central, the Recurrence Event, i.e., glacier advance following the LLGM in the western Massif Central (Sections 1 and 2.3), was correlated to the Grandvals stade in the Aubrac Mountains, despite uncertainties in moraine correlations (Kirkbride and Winkler, 2012).

Finally, the decay of the Aubrac plateau icefield (18.66±1.60 ka) was coeval with the onset of the HS-1 (18 to 15.6 ka; Sanchez Goñi and Harrison, 2010). This event was recognised as a receding glacier phase in the circum-Mediterranean mountains related to enhanced aridity (Allard et al., 2021). In the southwestern Massif Central, HS-1 was a period of glacier recession. In the Roustières section (Fig. 2), cold but arid conditions were reconstructed between 17.7 and 15 ka (Gandouin et al., 2016), while the Aubrac Mountains were probably deglaciated. Similar climatic conditions prevailed in the Cantal, the Cézallier and the Monts Dore deglaciated slopes (Ponel et al., 1991; Vergne, 1991; Miras et al., 2006). This is consistent with a radiocarbon age obtained in the northern Cantal on a kame terrace deposit (17.1–15.7 ka cal BP; calibrated with CLAM software v.2.3.2 and the "IntCal20" calibration curve; Blaauw, 2010; Reimer et al., 2020). This glacial deposit was deposited during the Cantal glacier recession (Veyret-Mekdjian et al., 1978) and supported glacier retreats in the Cantal during the HS1, as the Aubrac plateau icefield. At the beginning of Greenland Interstadial 1 (GI-1; at 14.7 ka; Rasmussen et al., 2014), a slight summer warming (+4°C, compared to Oldest Dryas temperature) was recorded at the Roustières site (Gandouin et al., 2016). This climatic amelioration was coeval with a general trend of slope stabilisation caused by the development of vegetation cover across the whole of the Massif Central (Fig. 9) (Reille and Beaulieu, 1988; Vergne, 1991; Degeai and Pastre, 2009; Gandouin et al., 2016; Ponel et al., 2016). These milder climatic conditions potentially led to glacier recession into higher elevation cirques of the Cantal and Monts Dore massifs (Veyret, 1978; Valadas, 1984; Vergne, 1991).

7 Conclusion

Five end moraines and one till in the Aubrac Mountains were selected, in accordance with field investigations, for surface exposure dating using ^{10}Be and ^{26}Al (n = 20). The new glacial chronology produced for the Aubrac plateau icefield southwestern Massif Central is in good agreement with (i) the existing morphostratigraphy previously established in the Aubrac Plateau and (ii) other paleoenvironmental records from the Massif Central and more widely in western Europe. The new data indicate that the LLGM occurred during the early part of MIS 2 (28–23 ka). It was followed by two glacier advances, referred to as Grandvals and Bouquincan stades, during GS-2.1 at 24–19 ka and 20–16 ka, respectively. The Aubrac plateau icefield decay is dated to GS-2.1a at 18–14 ka, in accordance with local paleoenvironmental data. The glacial chronology presented here is the first comprehensive chronological framework for the late Pleistocene glaciation in the French Massif Central. First, the LLGM in the Aubrac Mountains is synchronous with favourable conditions for glacier expansion in Central Europe (Alps) related to reduced North Atlantic circulation and enhanced moisture advection from the Mediterranean Sea that reached at least the southern Massif Central. Second, GS-2.1 in the Massif Central is characterised by a cold and arid climate with possible wetter climate phases that potentially led to two glacier advances: the Grandvals stade in the Aubrac Mountains (named the Recurrence Event in the Cantal, Cézallier and Monts Dore) and the Bouquincan stade in the Aubrac Mountains. These phases are associated with the potential northward shift of the westerlies. This may have trigged glacier advances in the Aubrac Mountains. Aridity during this period was the main limiting factor for glacier growth, especially during HS1, which is coeval with Aubrac plateau icefield decay and glacier retreat recorded in the north Cantal.

8 Acknowledgements

The first author received a PhD contract from the French Ministry of Higher Education, Research and Innovation. We thank the Laboratory Magma et Volcan, UMR 6524 CNRS/UCA for access to their laboratory facilities during cosmogenic exposure sample preparation. ^{10}Be and ^{26}Al analyses were performed at the ASTER AMS national facility (CEREGE, Aix-en-Provence), supported by the INSU/CNRS, by the ANR through the “Projets thématiques d’excellence” program for the

455 “Equipements d’excellence” ASTER-CEREGE action, and by the Institut de Recherche pour le
456 Développement (IRD). We also thank the ASTER Team (G. Aumaître, D. Bourlès, and K. Keddadouche)
457 for their AMS expertise. B. Chandler and an anonymous reviewer are warmly thanked for their
458 constructive comments and their help to improve this paper.

459

9 Tables

Table 1. Summary of key glacial landforms identified in the field fulfil criteria for cosmogenic exposure dating, with their significance in the existing morphostratigraphic framework for the Aubrac plateau icefield.

Local glacier stade		Glacial landform targeted for dating		
Local name	Field evidence	Geomorphological field survey	***Name*** (type of landform)	Location
Local Last Glacial Maximum	- in the Aubrac Plateau: maximum dispersion of erratic boulders, terminal moraines, - in Aubrac Valleys: maximum extent of glacially moulded morphologies and terminal moraine remnants.	*Veyret, 1978* *De Goër et al., 1994* *Poizat and Rousset, 1974* *Ancrenaz et al., 2020*	***Allatieux*** (end moraine)	Aubrac Plateau Rimeize watershed 1199 m
			Longevialle (end moraine)	Aubrac Plateau Bès valley 1040 m
Grandvals stade	- in the Aubrac Plateau: LLGM glacier melt-out sediments truncated by till and recessional moraines.	*Veyret, 1978* *Poizat, 1973* *Ancrenaz et al., 2020*	***Grandvals*** (end moraine)	Aubrac Plateau Bès valley 1059 m
			Rateylou (end moraine)	Aubrac Plateau Rimeize watershed 1185 m
Bouquincan stade	- in the Aubrac Plateau: Bouquincan recessional moraine.	*Ancrenaz et al., 2020*	***Bouquincan*** (end moraine)	Aubrac Plateau Bès valley 1157 m
Deglaciation	- in the Aubrac Highland: glacial deposits in the uppermost reaches of the Aubrac Valleys.	*Veyret, 1978* *De Goër et al., 1994* *Ancrenaz et al., 2020*	***Bonnecombe*** (glacial deposit)	Aubrac Highlands Doulounet valley 1345 m

Table 2. Location of the sampling sites and analytical data for Be-10 and Al-26 samples from the Aubrac Mountains.

Local glacier stade	*Landform & sample ID*	*Longitude*	*Latitude*	*Altitude (m a.s.l.)*	*Topographic schielding*	*Rock density ($g.cm^{-2}$)*	*Sample thickness (cm)*	*[^{10}Be] ($\times10^{-3}$ at.g^{-1})*	*[^{26}Al] ($\times10^{-3}$ at.g^{-1})*
	Allatieux moraine								
	AU16	3°13'52.9"	44°72'37.6"	1196	0.99	2.65	3.0	270.29 ± 7.6	1686.28 ± 192.2
	AU17	3°13'88.4"	44°72'12.9"	1192	0.99	2.65	2.0	266.75 ± 8.8	1559.80 ± 155.3
LLGM	***Longevialle moraine***								
	AU10	3°03'05.9"	44°76'50.7"	1039	0.99	2.65	2.0	230.70 ± 17.7	1343.50 ± 114.6
	AU11	3°02'93.8"	44°76'51.8"	1041	0.99	2.65	4.0	500.17 ± 17.5	2538.08 ± 125.0
	AU12	3°03'31.3"	44°76'50.8"	1036	0.99	2.65	4.0	176.16 ± 9.9	1156.15 ± 123.2
	Grandvals moraine								
	AU13	3°02'85.7"	44°74'24.9"	1055	0.99	2.65	3.0	202.19 ± 7.7	1257.79 ± 84.1
	AU14	3°02'88.4"	44°74'25.5"	1057	0.99	2.65	2.0	207.31 ± 10.8	804.75 ± 60.5
	AU15	3°02'86.9"	44°74'25.8"	1055	0.99	2.65	2.5	192.84 ± 8.7	1250.80 ± 95.9
	Rateylou isolated erratic boulder								
Grandvals stade	AU01	3°10'14.0"	44°69'77.4"	1195	0.99	2.65	3.5	107.28 ± 4.6	450.02 ± 47.5
	AU02	3°11'01.8"	44°69'74.7"	1192	0.99	2.65	3.0	228.22 ± 7.8	968.18 ± 75.0
	Rateylou moraine								
	AU03	3°10'93.0"	44°69'75.1"	1190	0.99	2.65	2.5	34.23 ± 2.7	159.10 ± 24.8
	AU04	3°10'93.1"	44°69'74.7"	1190	0.99	2.65	2.5	70.06 ± 4.2	393.36 ± 39.2
	AU05	3°11'17.3"	44°69'66.5"	1187	0.99	2.65	2.5	218.47 ± 9.1	1344.09 ± 72.1
	AU06	3°11'34.8"	44°69'61.6"	1183	0.99	2.65	3.0	207.74 ± 9.7	1087.26 ± 70.5
	Bouquincan moraine								
Bouquin-can stade	AU07	3°09'32.3"	44°66'15.5"	1158	0.99	2.65	4.0	172.94 ± 11.6	1051.46 ± 67.5
	AU08	3°09'25.3"	44°66'22.0"	1156	0.99	2.65	2.5	189.55 ± 8.4	1123.39 ± 76.2
	AU09	3°09'17.0"	44°66'25.4"	1153	0.99	2.65	3.5	75.28 ± 4.3	483.40 ± 85.2
	Bonnecombe till								
Deglacia-tion	AU31	3°12'28.1"	44°55'97.6"	1341	0.99	2.65	3.5	221.31 ± 7.2	n.a.
	AU32	3°12'65.9"	44°56'16.2"	1342	0.99	2.65	2.5	198.66 ± 6.7	n.a.
	AU33	3°12'66.5"	44°55'98.8"	1339	0.99	2.65	2.0	199.92 ± 7.9	n.a.

Table 3. Be-10 and Al-26 Minimum Exposure Age (MEA) results of samples from the Aubrac Mountains

Local glacier stade	*Landform & sample ID*	*$^{26}Al/^{10}Be$*	*^{10}Be MEA (ka)*	*^{26}Al MEA (ka)*	*Landform stabilization (uncert.-weighted mean in ka)*	*Landform age (oldest MEA in ka)*
LLGM	***Allatieux end moraine***					
	AU16	6.2 ± 0.7	25.41 ± 2.14	23.21 ± 3.62	24.29±1.28	25.41 ± 2.14
	AU17	5.8 ± 0.6	24.95 ± 2.15	21.34 ± 3.11		
	Longevialle end moraine					
	AU10	5.8 ± 0.7	24.31 ± 2.7	20.7 ± 2.81		
	AU11*	5.1 ± 0.3	53.86 ± 4.72	40.05 ± 4.7	n.a.	24.31 ± 2.7
	AU12	6.6 ± 0.8	18.88 ± 1.84	18.12 ± 2.72		
Grandvals stade	***Grandvals end moraine***					
	AU13	6.2 ± 0.5	21.22 ± 1.87	19.31 ± 2.41		
	AU14**	3.9 ± 0.4	21.55 ± 2.05	12.19 ± 1.57	20.43±0.93	21.55 ± 2.05
	AU15	6.5 ± 0.6	20.14 ± 1.84	19.11 ± 2.49		
	Rateylou isolated erratic boulders					
	AU01***	4.2 ± 0.5	10.09 ± 0.91	6.17 ± 0.92	n.a.	21.48 ± 1.86
	AU02	4.2 ± 0.4	21.48 ± 1.86	13.29 ± 1.73		
	Rateylou end moraine					
	AU03***	4.6 ± 0.8	3.2 ± 0.36	2.17 ± 0.41		
	AU04***	5.6 ± 0.7	6.55 ± 0.65	5.36 ± 0.77	19.68±1.11	20.55 ± 1.84
	AU05	6.2 ± 0.4	20.55 ± 1.84	18.49 ± 2.18		
	AU06	5.2 ± 0.4	19.67 ± 1.81	15.03 ± 1.86		
Bouquincan stade	***Bouquincan end moraine***					
	AU07	6.1 ± 0.6	16.83 ± 1.75	14.95 ± 1.84		
	AU08	5.9 ± 0.5	18.27 ± 1.66	15.82 ± 1.98	16.59±0.9	18.27 ± 1.66
	AU09***	6.4 ± 1.2	7.31 ± 0.72	6.84 ± 1.41		
Bonnecombe deposit	***Bonnecombe till***					
	AU31	n.a.	18.66 ± 1.6	n.a.		
	AU32	n.a.	16.6 ± 1.43	n.a.	17.23±0.87	18.66 ± 1.6
	AU33	n.a.	16.68 ± 1.48	n.a.		

* MEA rejected for the uncertainty weighted-mean calculation and interpreted as prior-exposure; ** Al-26 MEA rejected for the uncertainty-weighted mean calculation; *** MEA rejected for the uncertainty-weighted mean calculation and interpreted as incomplete exposure age

10 Figure captions

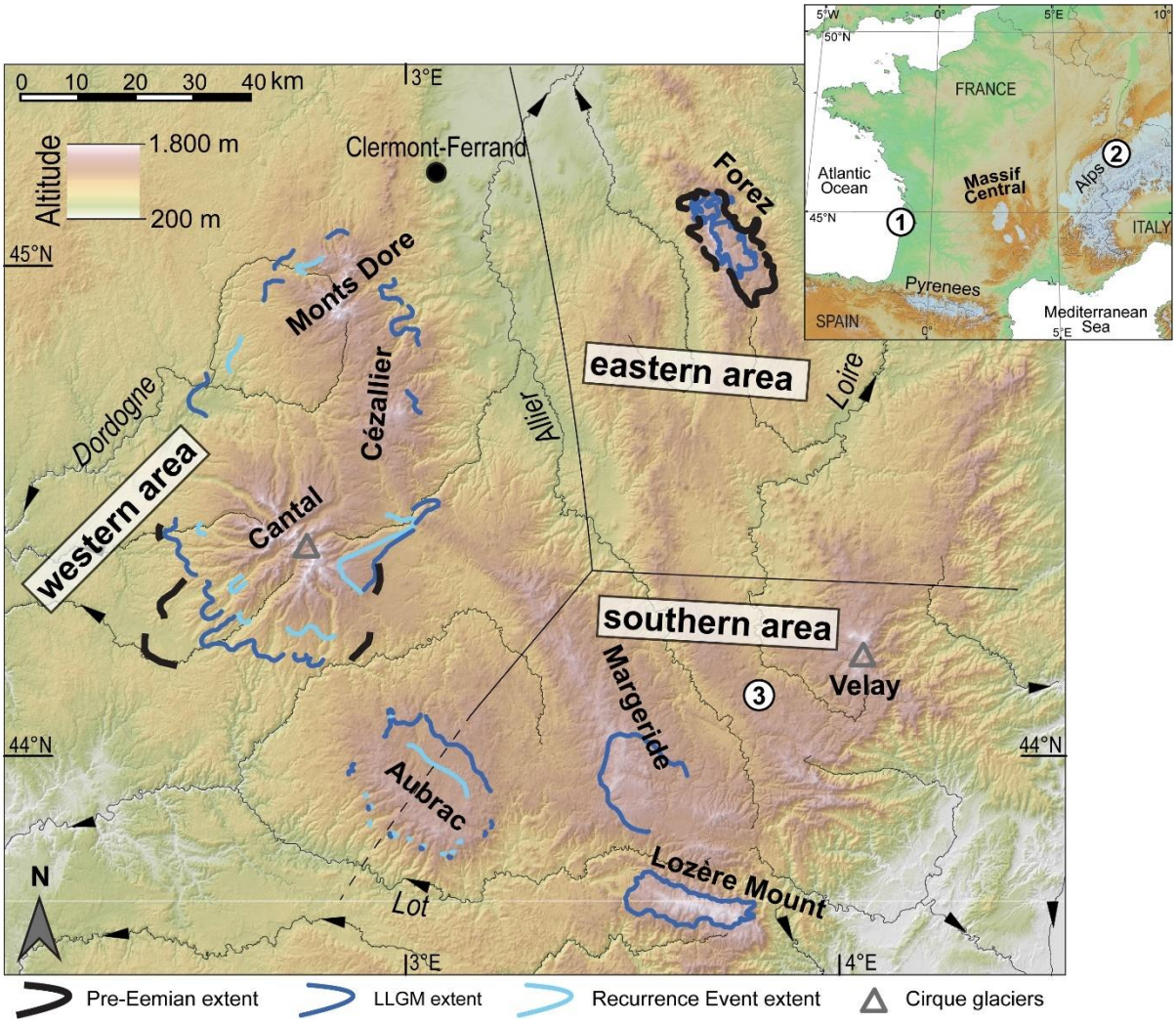

Figure 1. Extent and chronology of late Pleistocene glaciation in the Massif Central (Etlicher and De Goër, 1988) and the three groups of glaciated areas according to Veyret (1978). Localities cited in the main text are as follows: 1, the Aquitaine Basin; 2, the Sieben Hengste Cave 7H speleothem record (Luetscher et al., 2015); and 3, the Lake Bouchet pollen sequence (Reille and Beaulieu, 1988).

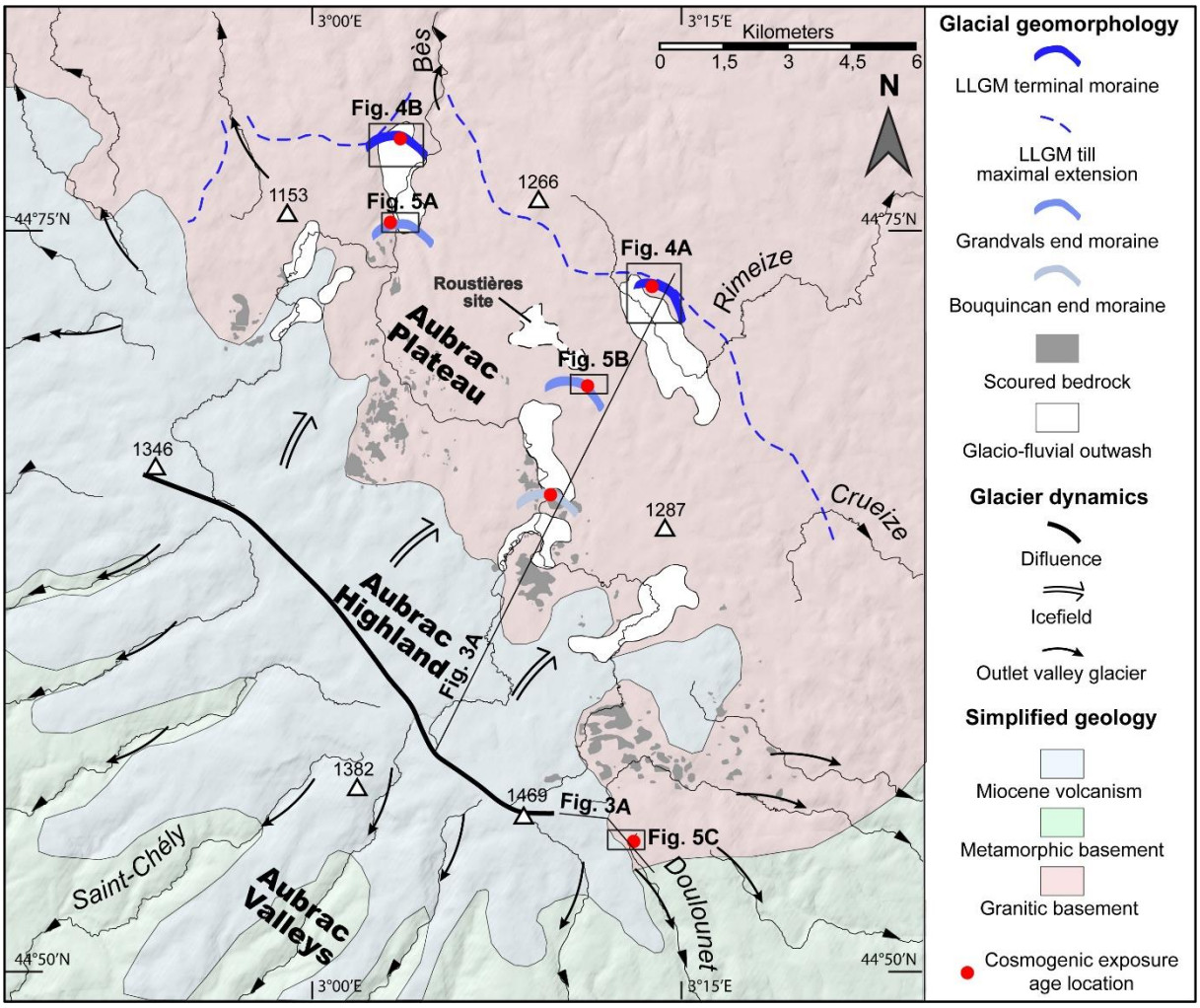

Figure 2. Aubrac Mountains lithostructural context and glacial geomorphology, with the location of sample sites for cosmogenic exposure age dating.

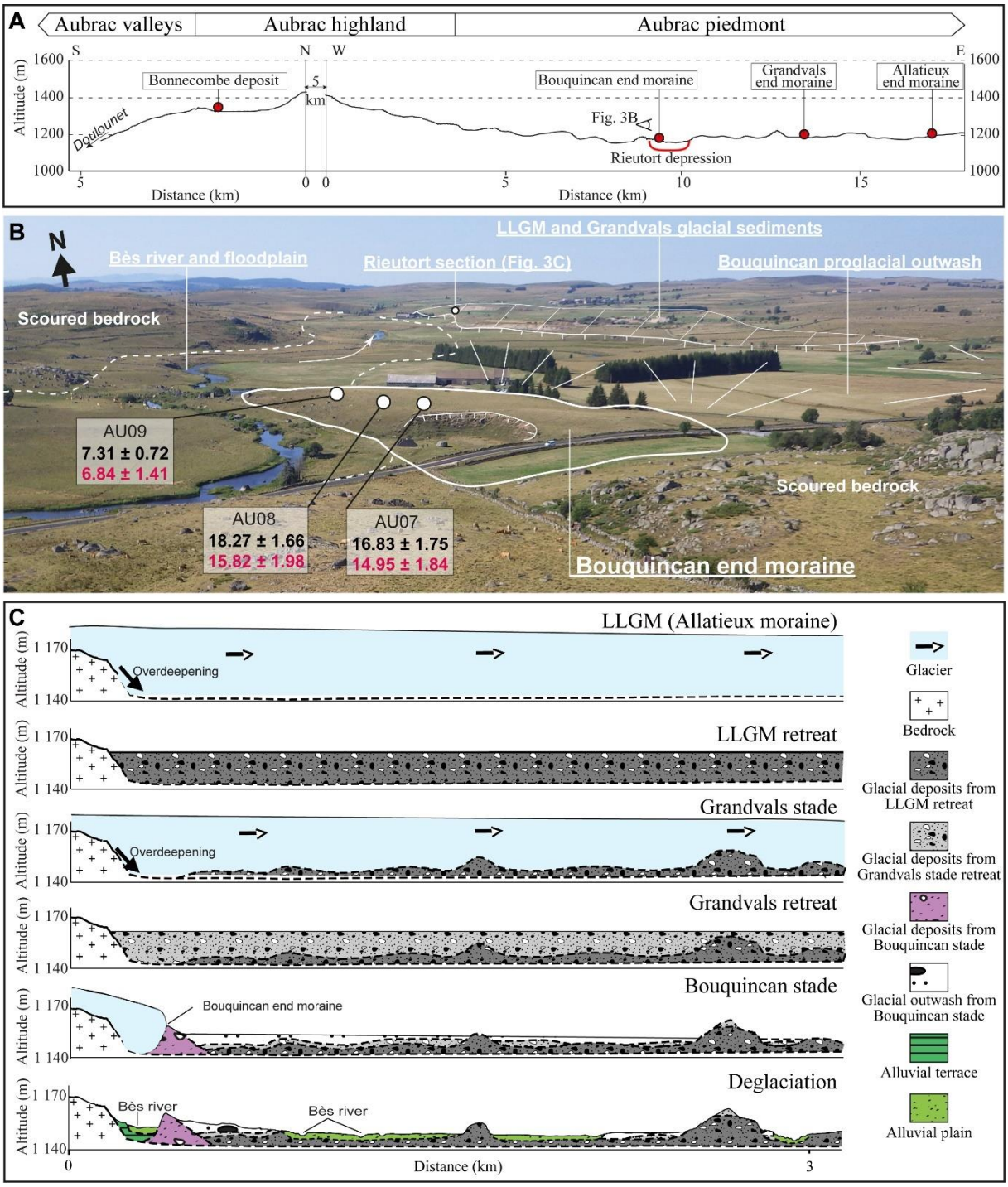

Figure 3. Locations of the main glacial landforms and sediments in the Aubrac Mountains from which the morphostratigraphic framework was built. A) Topographic profile from south to east across the Aubrac Mountains showing the locations of ice-marginal landforms and dated glacial deposits. For the location of the profiles, see Fig. 2. B) Annotated photograph of the glacial landform assemblages identified in the Rieutort depression (Poizat, 1973; Veyret, 1978; Ancrenaz et al., 2020). The upper (black) and lower (red) ages refer to ^{10}Be and ^{26}Al minimum exposure ages, respectively. C) Glacial

fluctuations reconstructed from the stratigraphic assemblages from the Rieutort section, located in the Rieutort depression (modified from Ancrenaz et al., 2020).

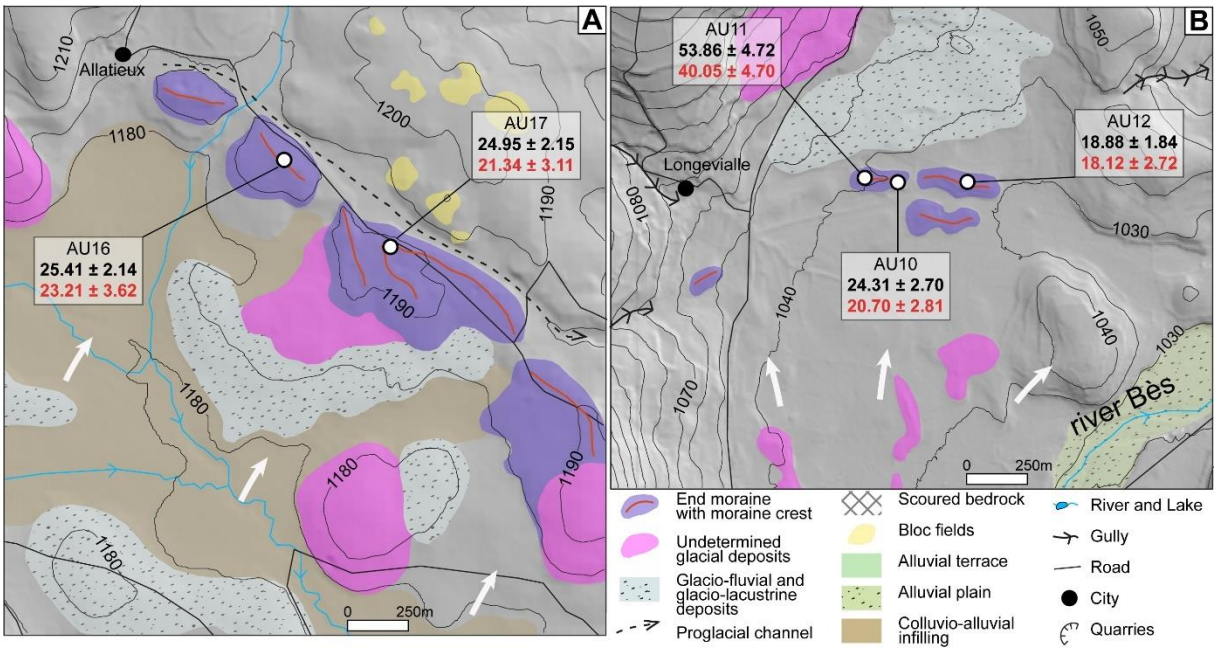

488

489 **Figure 4.** Geomorphological settings of (A) the Allatieux and (B) Longevialle end moraines, with the
490 locations of sampled moraine boulders. Upper (black) and lower (red) ages refer to ^{10}Be and ^{26}Al
491 MEAs, respectively, with their uncertainty (analytical and production rate). White arrows indicate the
492 direction of the glacier flow. For the location of the captions, see Fig. 2.

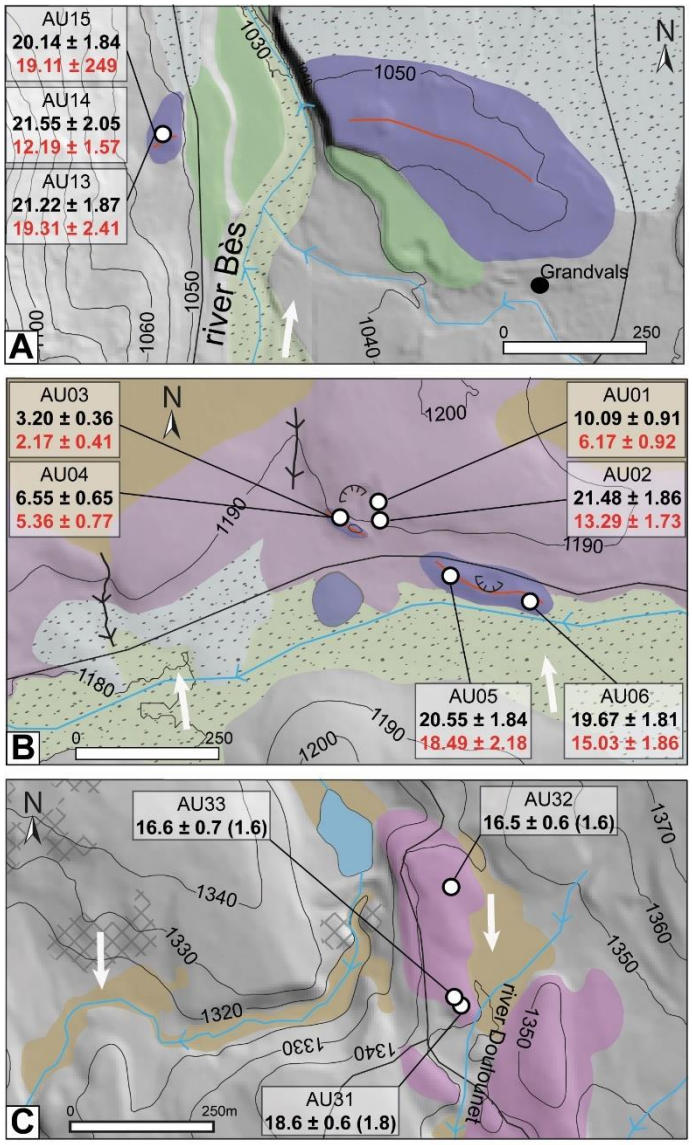

493

494 **Figure 5.** Geomorphological settings of (A) the Grandvals end moraine, (B) the Rateylou end moraine
495 and associated isolated boulders and (C) the Bonnecombetill, with sample locations of morainic
496 boulders. Upper (black) and lower (red) ages refer to ^{10}Be and ^{26}Al MEAs, respectively, with their
497 uncertainty (analytical and production rate). White arrows indicate the direction of glacier flow.. For
498 the location of the captions, see Fig. 2. Same legend as that for Fig. 4.

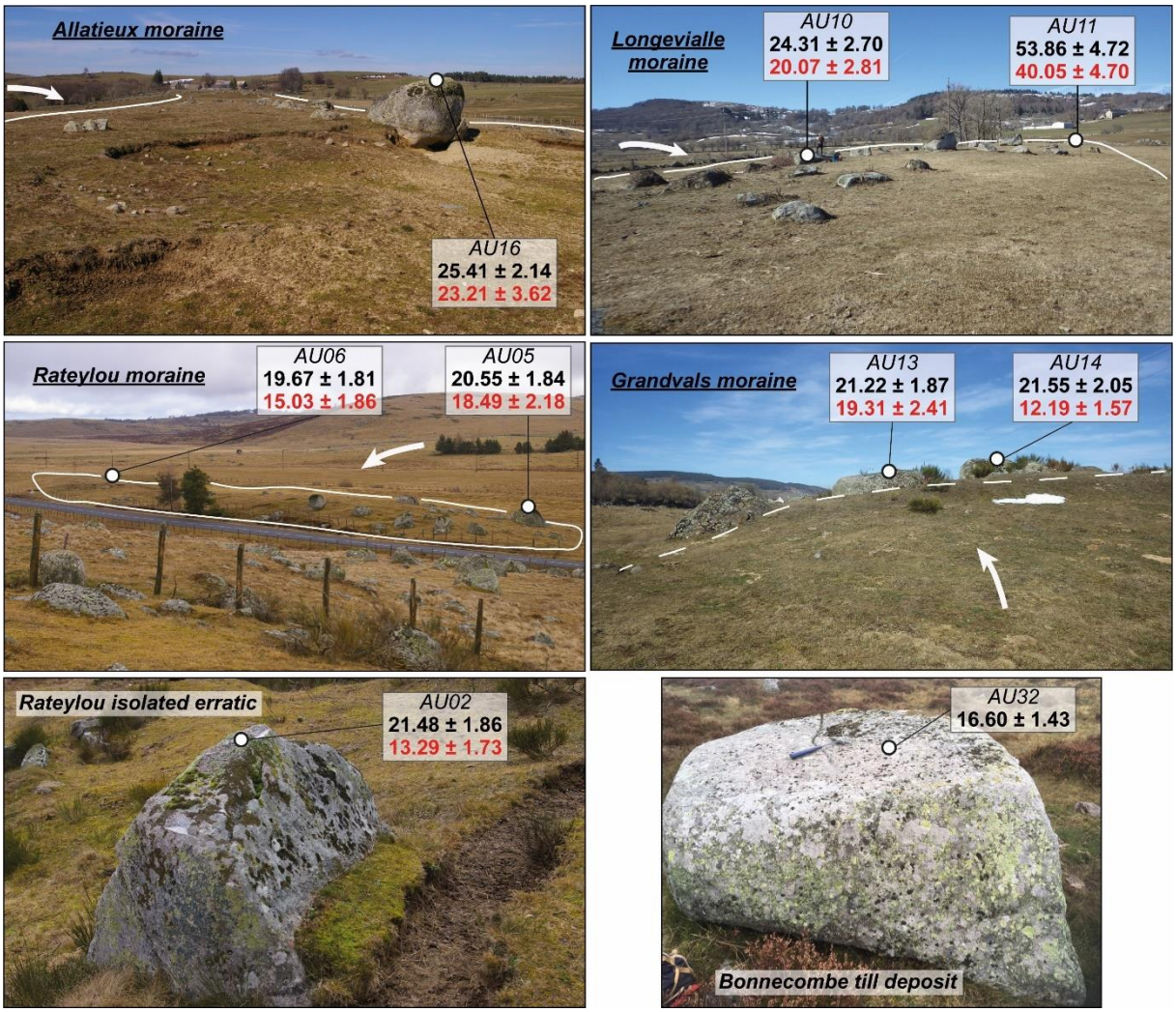

Figure 6. Photographs of sampled granitic erratic boulders embedded in glacial landforms in the Aubrac Mountains. Only sample AU02 is collected from an isolated erratic boulder. The upper (black) and lower (red) ages refer to ^{10}Be and ^{26}Al minimum exposure ages, respectively. Glacier flow is indicated by the white arrows.

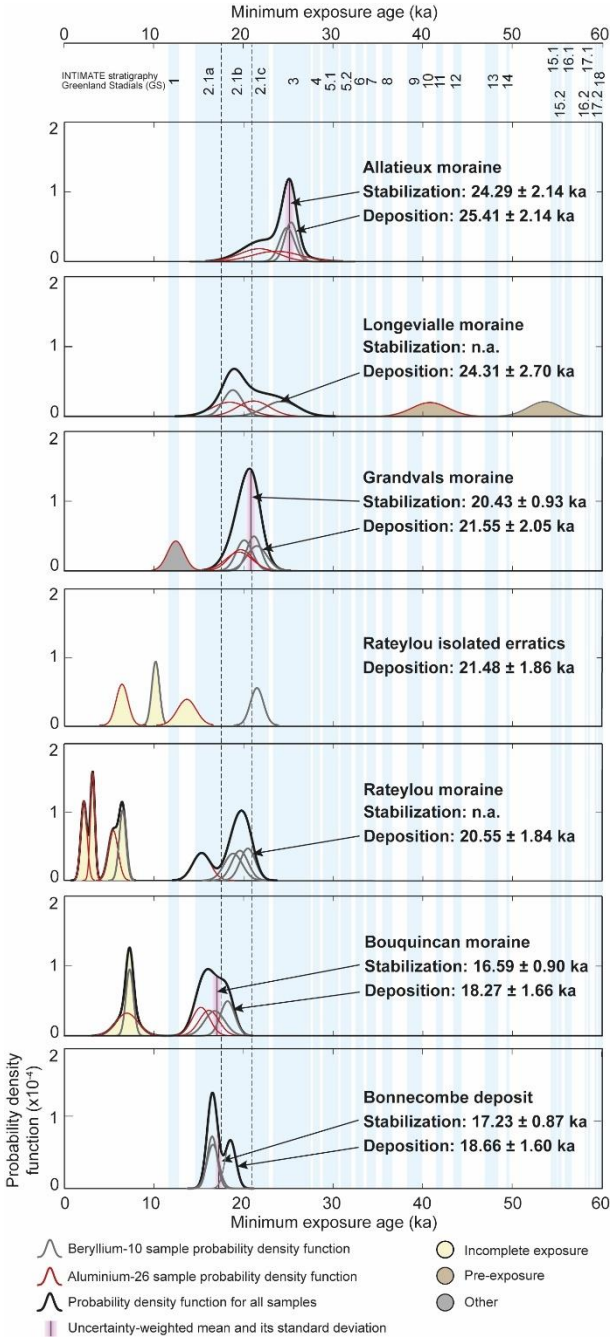

Figure 7. Probability density function of MEAs by location versus stadials from the INTIMATE stratigraphy (Rasmussen et al., 2014). The landform age is inferred from the oldest MEA that is not rejected by the X_R^2 test (Section 6.1). Only the internal uncertainty is shown.

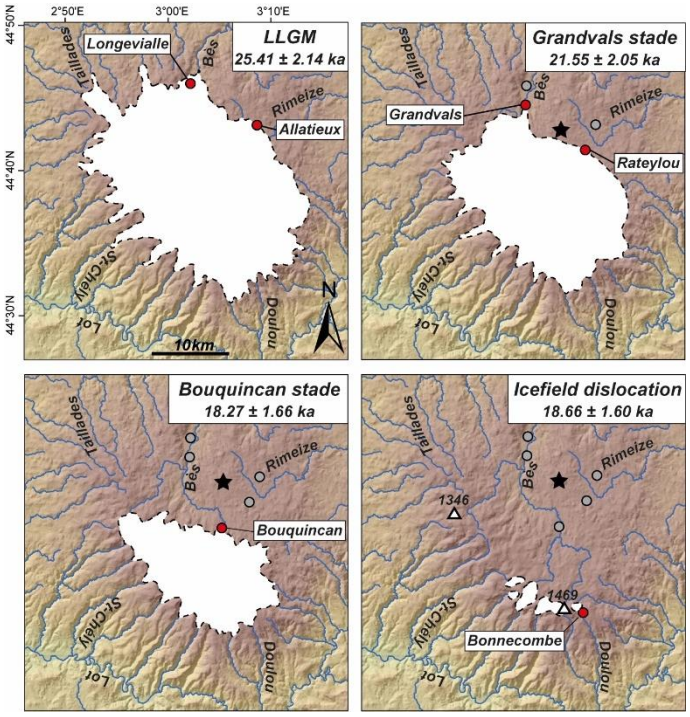

Figure 8. Diachronic reconstructions of the Aubrac plateau icefield extent during MIS 2. Red dots are glacial landforms whose exposure ages indicate the minimum age of deglaciation. Glacial limits are uncertain and based on geomorphological (subglacially moulded morphologies and topographic constraints) and sedimentological observations (extension of till) (Poizat and Rousset, 1975; Veyret, 1978; Ancrenaz et al., 2020). The black star represents the location of the Roustière site (Gandouin et al., 2016; Ponel et al., 2016); note that it is located inside the LLGM outer limit (see Section 2.3 for further details).

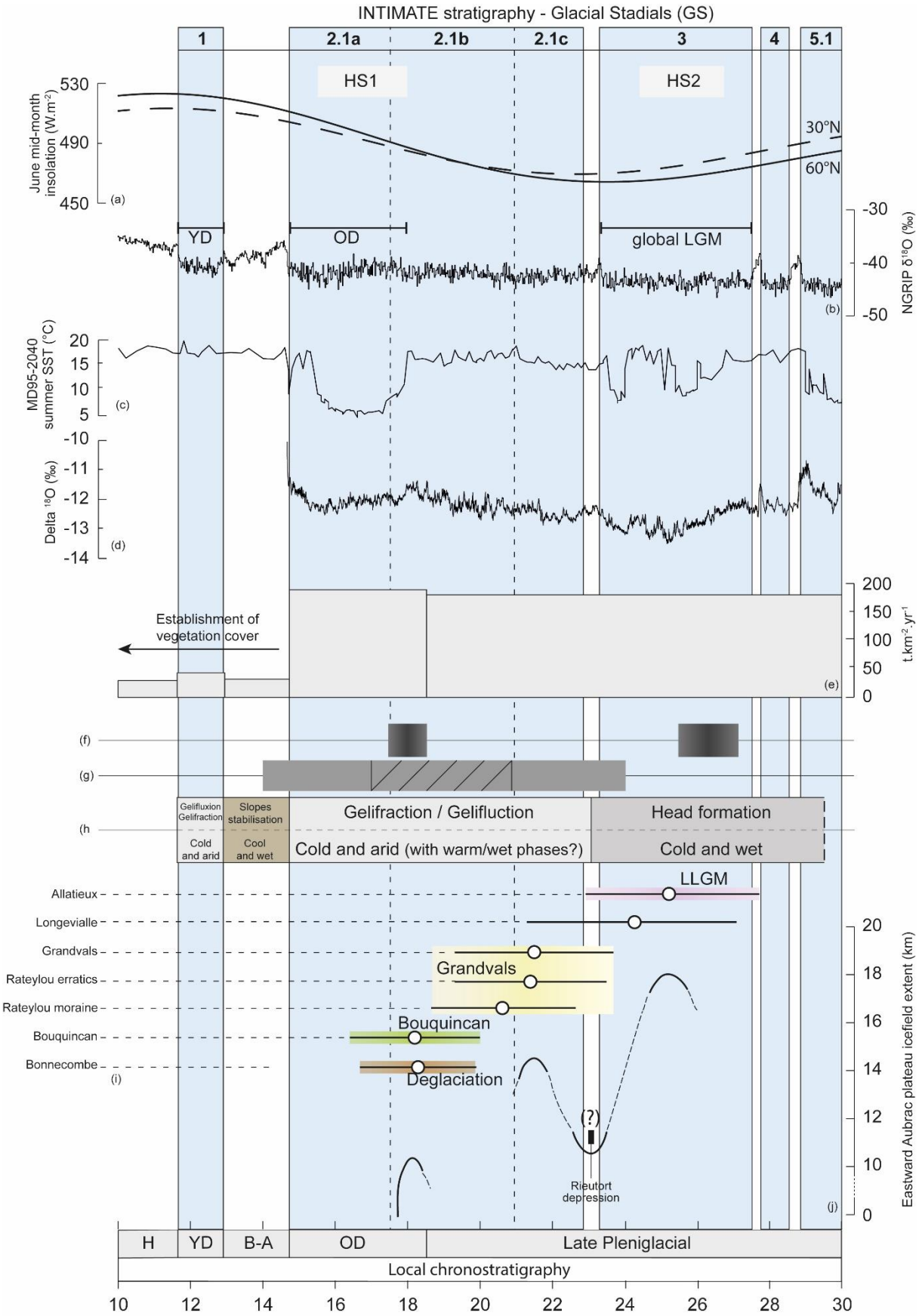

516

517 **Figure 9.** Synthetic chronological framework for the southwestern Massif Central against main

paleoenvironmental proxies cited in the main text. a) June mid-month insolation in $W.m^{-2}$ at 60°N (black line) at 30°N (dashed line) (Berger and Loutre, 1991), b) North Greenland Ice Core Project (NGRIP) $\delta^{18}O$ from the Greenland ice core (Rasmussen et al., 2014). c) Summer Sea Surface Temperature (SST) reconstructed from the MD95-2040 oceanic sediment core from the western Iberian Margin (Salgueiro et al., 2010). d) Sieben Hengste $\delta^{18}O$ record (Luetscher et al., 2015). e) Erosion rate in the Lake Bouchet watershed (Degeai and Pastre, 2009). f) Timing of episodes of permafrost in southwestern France (Lenoble et al., 2012; Bertran et al., 2014). g) Timing of aeolian sand cover accumulation in the Aquitaine Bassin (southwestern France). The dashed part corresponds to period of reduced aeolian activity related to permafrost degradation (Sitzia et al., 2015). h) Resumed stratigraphic chronology for the Massif Central nonglaciated slopes (Van Vliet-Lanoë et al., 1991). i) Ages of glacial landforms in the Aubrac Mountains according to exposure ages for erratic boulders (this study). j) Reconstructed extension of the eastern part of the Aubrac plateau icefield. For the boundaries of the LGM, the Oldest Dryas (OD), the Younger Dryas (YD) and of the Heinrich Stadials 1 and 2 (HS-1 and -2), see Hughes and Gibbard (2015), Shakun and Carlson (2010), Carlson (2013) and Sanchez Goñi and Harrison (2010), respectively.

11 References

Allard, J.L., Hughes, P.D., Woodward, J.C., 2021. Heinrich Stadial aridity forced Mediterranean-wide glacier retreat in the last cold stage. Nat. Geosci. 14, 197–205. https://doi.org/10.1038/s41561-021-00703-6

Allard, J.L., Hughes, P.D., Woodward, J.C., Fink, D., Simon, K., Wilcken, K.M., 2020. Late Pleistocene glaciers in Greece: A new 36Cl chronology. Quaternary Science Reviews 245, 106528. https://doi.org/10.1016/j.quascirev.2020.106528

Ancrenaz, A., Define, E., Poiraud, A., 2020. Fluctuations glaciaires au Pléistocène supérieur dans les Monts d'Aubrac (Massif central, France) : nouvelles données. Géomorphologie : relief, processus, environnement 26, 16. https://doi.org/10.4000/geomorphologie.14516

Applegate, P.J., Urban, N.M., Keller, K., Lowell, T.V., Laabs, B.J.C., Kelly, M.A., Alley, R.B., 2012. Improved moraine age interpretations through explicit matching of geomorphic process models to cosmogenic nuclide measurements from single landforms. Quaternary Research 77, 293–304. https://doi.org/10.1016/j.yqres.2011.12.002

Arnold, M., Merchel, S., Bourlès, D.L., Braucher, R., Benedetti, L., Finkel, R.C., Aumaître, G., Gottdang, A., Klein, M., 2010. The French accelerator mass spectrometry facility ASTER: Improved performance and developments. Nuclear Instruments and Methods in Physics Research Section B: Beam Interactions with Materials and Atoms, 19th International Conference on Ion Beam Analysis 268, 1954–1959. https://doi.org/10.1016/j.nimb.2010.02.107

Balco, G., 2011. Contributions and unrealized potential contributions of cosmogenic-nuclide exposure dating to glacier chronology, 1990–2010. Quaternary Science Reviews 30, 3–27. https://doi.org/10.1016/j.quascirev.2010.11.003

Bertran, P., Andrieux, E., Antoine, P., Coutard, S., Deschodt, L., Gardère, P., Hernandez, M., Legentil, C., Lenoble, A., Liard, M., Mercier, N., Moine, O., Sitzia, L., Van Vliet-Lanoë, B., 2014. Distribution and chronology of Pleistocene permafrost features in France: Database and first results: Pleistocene permafrost features in France. Boreas 43, 699–711. https://doi.org/10.1111/bor.12025

Borchers, B., Marrero, S., Balco, G., Caffee, M., Goehring, B., Lifton, N., Nishiizumi, K., Phillips, F., Schaefer, J., Stone, J., 2016. Geological calibration of spallation production rates in the CRONUS-Earth project. Quaternary Geochronology 31, 188–198. https://doi.org/10.1016/j.quageo.2015.01.009

Boston, C.M., Lukas, S., Carr, S.J., 2015. A Younger Dryas plateau icefield in the Monadhliath, Scotland, and implications for regional palaeoclimate. Quaternary Science Reviews 108, 139–162. https://doi.org/10.1016/j.quascirev.2014.11.020

Braucher, R., Guillou, V., Bourlès, D.L., Arnold, M., Aumaître, G., Keddadouche, K., Nottoli, E., 2015. Preparation of ASTER in-house 10Be/9Be standard solutions. Nuclear Instruments and Methods in Physics Research Section B: Beam Interactions with Materials and Atoms, The Thirteenth Accelerator Mass Spectrometry Conference 361, 335–340. https://doi.org/10.1016/j.nimb.2015.06.012

Braucher, R., Merchel, S., Borgomano, J., Bourlès, D.L., 2011. Production of cosmogenic radionuclides at great depth: A multi element approach. Earth and Planetary Science Letters 309, 1–9. https://doi.org/10.1016/j.epsl.2011.06.036

Briner, J.P., Kaufman, D.S., Manley, W.F., Finkel, R.C., Caffee, M.W., 2005. Cosmogenic exposure dating of late Pleistocene moraine stabilization in Alaska. Geol Soc America Bull 117, 1108. https://doi.org/10.1130/B25649.1

Brown, E.T., Edmond, J.M., Raisbeck, G.M., Yiou, F., Kurz, M.D., Brook, E.J., 1991. Examination of surface exposure ages of Antarctic moraines using in situ produced 10Be and 26Al. Geochimica et Cosmochimica Acta 55, 2269–2283. https://doi.org/10.1016/0016-7037(91)90103-C

Calvet, M., Delmas, M., Gunnell, Y., Braucher, R., Bourlès, D., 2011. Recent Advances in Research on Quaternary Glaciations in the Pyrenees, in: Developments in Quaternary Sciences. Elsevier, pp. 127–139. https://doi.org/10.1016/B978-0-444-53447-7.00011-8

Chevalier, M.-L., Hilley, G., Tapponnier, P., Van Der Woerd, J., Liu-Zeng, J., Finkel, R.C., Ryerson, F.J., Li, H., Liu, X., 2011. Constraints on the late Quaternary glaciations in Tibet from cosmogenic exposure ages of moraine surfaces. Quaternary Science Reviews 30, 528–554. https://doi.org/10.1016/j.quascirev.2010.11.005

Chevalier, M.-L., Replumaz, A., 2019. Deciphering old moraine age distributions in SE Tibet showing bimodal climatic signal for glaciations: Marine Isotope Stages 2 and 6. Earth and Planetary Science Letters 507, 105–118. https://doi.org/10.1016/j.epsl.2018.11.033

Chmeleff, J., von Blanckenburg, F., Kossert, K., Jakob, D., 2010. Determination of the 10Be half-life by multicollector ICP-MS and liquid scintillation counting. Nuclear Instruments and Methods in Physics Research Section B: Beam Interactions with Materials and Atoms 268, 192–199. https://doi.org/10.1016/j.nimb.2009.09.012

Couturié, J.-P., 1977. Le massif granitique de la Margeride (Massif Central Français). Univ. Clermont II.

Defive, E., Raynal, J.P., Ancrenaz, A., Poiraud, A., 2019. L'englacement quaternaire du Massif central, in: Histoire de la découverte géologique du Massif central français, Mémoire. Société d'Histoire Naturelle d'Auvergne, p. 267.

Degeai, J.-P., Pastre, J.-F., 2009. Impacts environnementaux sur l'érosion des sols au Pléistocène supérieur et à L'holocène dans le cratère de maar du lac du Bouchet (Massif central, France). quaternaire 149–159. https://doi.org/10.4000/quaternaire.5101

Delmas, M., 2015. The last maximum ice extent and subsequent deglaciation of the Pyrenees: an overview of recent research. Cuadernos de Investigación Geográfica 41, 359. https://doi.org/10.18172/cig.2708

Delmas, M., Calvet, M., Gunnell, Y., Braucher, R., Bourlès, D., 2011. Palaeogeography and 10Be exposure-age chronology of Middle and Late Pleistocene glacier systems in the northern Pyrenees: Implications for reconstructing regional palaeoclimates. Palaeogeography, Palaeoclimatology, Palaeoecology 305, 109–122. https://doi.org/10.1016/j.palaeo.2011.02.025

Domínguez-Villar, D., Carrasco, R.M., Pedraza, J., Cheng, H., Edwards, R.L., Willenbring, J.K., 2013. Early maximum extent of paleoglaciers from Mediterranean mountains during the last glaciation. Sci Rep 3, 2034. https://doi.org/10.1038/srep02034

Etlicher, B., 1986. Les massifs du Forez, du Pilat et du Vivarais : régionalisation et dynamique des héritages glaciaires et périglaciaires en moyenne montagne cristalline. Univ. Saint-Etienne, Jean Monnet.

Etlicher, B., Goër de Hervé, A. (de), 1988. La déglaciation würmienne dans le Massif Central français, le point des travaux récents / The Würmian déglaciation in the French Massif-Central, review of recent works,. Bulletin de l'Association française pour l'étude du quaternaire 25, 103–110. https://doi.org/10.3406/quate.1988.1871

Etlicher, B., Van Leeuwen, J.F.N., Janssen, C.R., Juvigné, E., 1987. Le Haut Forez (Massif Central, France) après le pléniglaciaire würmien : environnement et tephra du volcan de La Nugère. Bulletin de l'Association française pour l'étude du quaternaire 24, 229–239. https://doi.org/10.3406/quate.1987.1852

Faure, É., 2012. "'Hautes terres'": l'anthropisation des monts d'Aubrac et du Lévezou (Massif Central, France) durant l'holocène: approche palynologique des dynamiques socio-environnementales en moyenne montagne. Univ. Le Mirail (Toulouse II).

Florineth, D., Schlüchter, C., 2000. Alpine Evidence for Atmospheric Circulation Patterns in Europe during the Last Glacial Maximum. Quat. res. 54, 295–308. https://doi.org/10.1006/qres.2000.2169

Gandouin, E., Rioual, P., Pailles, C., Brooks, S.J., Ponel, P., Guiter, F., Djamali, M., Andrieu-Ponel, V., Birks, H.J.B., Leydet, M., Belkacem, D., Haas, J.N., Van der Putten, N., de Beaulieu, J.L., 2016. Environmental and climate reconstruction of the late-glacial-Holocene transition from a lake sediment sequence in Aubrac, French Massif Central: Chironomid and diatom evidence. Palaeogeography, Palaeoclimatology, Palaeoecology 461, 292–309. https://doi.org/10.1016/j.palaeo.2016.08.039

Gillespie, A., Molnar, P., 1995. Asynchronous maximum advances of mountain and continental glaciers. Reviews of Geophysics 33, 311. https://doi.org/10.1029/95RG00995

Goër de Hervé, A. (de), 1972. La Planèze de Saint-Flour : structure et géomorphologie glaciaire. Univ. Clermont II.

Goër de Hervé, A. (de), Baubron, J.-C., Cantagrel, J.-M., Makhoul, J., 1991. Le volcanisme de l'Aubrac (Massif central) : un bref épisode basaltique (250 000 ans) au Miocène supérieur (7,5 Ma). Géologie de la France 3–14.

Goër de Hervé, A. (de), Briand, B., Couturié, J.-P., Delpuech, A., Doche, B., Makhoul, J., Mercier-Batard, F., Michaëly, B., 1994. Notice explicative, Carte géol. France (1/50 000), feuille Nasbinals (837).

Gribenski, N., Valla, P.G., Preusser, F., Roattino, T., Crouzet, C., Buoncristiani, J.-F., 2021. Out-of-phase Late Pleistocene glacial maxima in the WesternAlps reflect past changes in North Atlantic atmospheric circulation. Geology. https://doi.org/10.1130/G48688.1

Heyman, J., Applegate, P.J., Blomdin, R., Gribenski, N., Harbor, J.M., Stroeven, A.P., 2016. Boulder height – exposure age relationships from a global glacial 10Be compilation. Quaternary Geochronology 34, 1–11. https://doi.org/10.1016/j.quageo.2016.03.002

Heyman, J., Stroeven, A.P., Harbor, J.M., Caffee, M.W., 2011. Too young or too old: Evaluating cosmogenic exposure dating based on an analysis of compiled boulder exposure ages. Earth and Planetary Science Letters 302, 71–80. https://doi.org/10.1016/j.epsl.2010.11.040

Hughes, A.L.C., Gyllencreutz, R., Lohne, Y.S., Mangerud, J., Inge, J., 2015. The last Eurasian ice sheets – a chronological database and time-slice reconstruction 67. https://doi.org/10.1111/bor.12142

Hughes, P.D., Gibbard, P.L., 2015. A stratigraphical basis for the Last Glacial Maximum (LGM). Quaternary International 383, 174–185. https://doi.org/10.1016/j.quaint.2014.06.006

Hughes, P.D., Gibbard, P.L., Ehlers, J., 2013. Timing of glaciation during the last glacial cycle: evaluating the concept of a global 'Last Glacial Maximum' (LGM). Earth-Science Reviews 125, 171–198. https://doi.org/10.1016/j.earscirev.2013.07.003

Hughes, P.D., Woodward, J.C., 2017. Quaternary glaciation in the Mediterranean mountains: a new synthesis. Geological Society, London, Special Publications 433, 1–23. https://doi.org/10.1144/SP433.14

Jorda, M., Rosique, T., Évin, J., 2000. Données nouvelles sur l'âge du dernier maximum glaciaire dans les Alpes méridionales françaises. Comptes Rendus de l'Académie des Sciences - Series IIA - Earth and Planetary Science 331, 187–193. https://doi.org/10.1016/S1251-8050(00)01408-7

Jubertie, F., 2006. Les excès climatiques dans le Massif central français. L'impact des temps forts pluviométriques et anémométriques en Auvergne. Université Blaise Pascal - Clermont Ferrand II.

Kageyama, M., Nebout, N.C., Sepulchre, P., Peyron, O., Krinner, G., Ramstein, G., Cazet, J.-P., 2005. The Last Glacial Maximum and Heinrich Event 1 in terms of climate and vegetation around the Alboran Sea: a preliminary model-data comparison. Comptes Rendus Geoscience 337, 983–992. https://doi.org/10.1016/j.crte.2005.04.012

Kirkbride, M.P., Winkler, S., 2012. Correlation of Late Quaternary moraines: impact of climate variability, glacier response, and chronological resolution. Quaternary Science Reviews 46, 1–29. https://doi.org/10.1016/j.quascirev.2012.04.002

Kleman, J., Borgström, I., 1996. Reconstruction of palaeo-ice sheets: the use of geomorphological data. Earth Surface Processes and Landforms 21, 893–909. https://doi.org/10.1002/(SICI)1096-9837(199610)21:10<893::AID-ESP620>3.0.CO;2-U

Korschinek, G., Bergmaier, A., Faestermann, T., Gerstmann, U.C., Knie, K., Rugel, G., Wallner, A., Dillmann, I., Dollinger, G., von Gostomski, Ch.L., Kossert, K., Maiti, M., Poutivtsev, M., Remmert, A., 2010. A new value for the half-life of 10Be by Heavy-Ion Elastic Recoil Detection and liquid scintillation counting. Nuclear Instruments and Methods in Physics Research Section B: Beam Interactions with Materials and Atoms 268, 187–191. https://doi.org/10.1016/j.nimb.2009.09.020

Kuhlemann, J., Rohling, E.J., Krumrei, I., Kubik, P., Ivy-Ochs, S., Kucera, M., 2008. Regional Synthesis of Mediterranean Atmospheric Circulation During the Last Glacial Maximum. Science 321, 1338–1340. https://doi.org/10.1126/science.1157638

Laville, H., Raynal, J.P., Texier, J.P., 1986. Le dernier interglaciaire et le cycle climatique würmien dans le Sud-Ouest et le Massif Central Français. Bulletin de l'Association française pour l'étude du quaternaire 23, 35–46. https://doi.org/10.3406/quate.1986.1791

Lécuyer, C., Hillaire-Marcel, C., Burke, A., Julien, M.-A., Hélie, J.-F., 2021. Temperature and precipitation regime in LGM human refugia of southwestern Europe inferred from δ13C and δ18O of large mammal remains. Quaternary Science Reviews 255, 106796. https://doi.org/10.1016/j.quascirev.2021.106796

Leibrandt, S., 2011. Reconstitution de l'évolution morpho-structurale et de la dynamique éruptive du massif du Cantal: relation avec la distribution spatio-temporelle du volcanisme du Massif Central (France). Univ. Paris Sud 2.

Lenoble, A., Bertran, P., Mercier, N., Sitzia, L., 2012. Le site du Lac Bleu et la question de l'extension du pergélisol en France au Pléistocène supérieur 18.

Livingstone, S.J., Evans, D.J.A., Ó Cofaigh, C., Hopkins, J., 2010. The Brampton kame belt and Pennine escarpment meltwater channel system (Cumbria, UK): Morphology, sedimentology and formation. Proceedings of the Geologists' Association, Quaternary Geology of the British Isles: Part 2 121, 423–443. https://doi.org/10.1016/j.pgeola.2009.10.005

Lisiecki, L.E., Raymo, M.E., 2005. A Pliocene-Pleistocene stack of 57 globally distributed benthic δ18O records. Paleoceanography 20. https://doi.org/10.1029/2004PA001071

Lovell, H., Livingstone, S.J., Boston, C.M., Booth, A.D., Storrar, R.D., Barr, I.D., 2019. Complex kame belt morphology, stratigraphy and architecture. Earth Surf. Process. Landforms 44, 2685–2702. https://doi.org/10.1002/esp.4696

Ludwig, P., Shao, Y., Kehl, M., Weniger, G.-C., 2018. The Last Glacial Maximum and Heinrich event I on the Iberian Peninsula: A regional climate modelling study for understanding human settlement patterns. Global and Planetary Change 170, 34–47. https://doi.org/10.1016/j.gloplacha.2018.08.006

Luetscher, M., Boch, R., Sodemann, H., Spötl, C., Cheng, H., Edwards, R.L., Frisia, S., Hof, F., Müller, W., 2015. North Atlantic storm track changes during the Last Glacial Maximum recorded by Alpine speleothems. Nat Commun 6, 6344. https://doi.org/10.1038/ncomms7344

Manley, G., 1955. On the Occurrence of Ice Domes and Permanently Snow-Covered Summits. Journal of Glaciology 2, 453–456. https://doi.org/10.3189/002214355793702244

Meierding, T.C., 1982. Late pleistocene glacial equilibrium-line altitudes in the Colorado Front Range: A comparison of methods. Quaternary Research 18, 289–310. https://doi.org/10.1016/0033-5894(82)90076-X

Merchel, Herpers, 1999. An Update on Radiochemical Separation Techniques for the Determination of Long-Lived Radionuclides via Accelerator Mass Spectrometry. ract 84, 215. https://doi.org/10.1524/ract.1999.84.4.215

Merchel, S., Arnold, M., Aumaître, G., Benedetti, L., Bourlès, D.L., Braucher, R., Alfimov, V., Freeman, S.P.H.T., Steier, P., Wallner, A., 2008. Towards more precise 10Be and 36Cl data from measurements at the 10−14 level: Influence of sample preparation. Nuclear Instruments and Methods in Physics Research Section B: Beam Interactions with Materials and Atoms 266, 4921–4926. https://doi.org/10.1016/j.nimb.2008.07.031

Miras, Y., Guenet, P., 2013. Une histoire plurimillénaire des paysages du Cézallier et ses liens avec les activités agrosylvopastorales depuis le Néolithique à partir de l'analyse pollinique de la tourbière de La Borie (1170 m, Saint-Saturnin, Cantal) 17.

Monegato, G., Ravazzi, C., Donegana, M., Pini, R., Calderoni, G., Wick, L., 2007. Evidence of a two-fold glacial advance during the last glacial maximum in the Tagliamento end moraine system (eastern Alps). Quat. res. 68, 284–302. https://doi.org/10.1016/j.yqres.2007.07.002

Monegato, G., Scardia, G., Hajdas, I., Rizzini, F., Piccin, A., 2017. The Alpine LGM in the boreal ice-sheets game. Sci Rep 7, 2078. https://doi.org/10.1038/s41598-017-02148-7

Palacios, D., Gomez-Ortiz, A., Alcala, J., Andrès, N., Oliva, M., Tanarro, L.M., Franch, F.S., Schimmelpfennig, I., Fernandz-Fernandez, J.M., Léanni, L., Aster Team, 2019. The challenging application of cosmogenic dating methods in residual glacial landforms: the case of Sierra Nevada (Spain) Geomorphology, 103–118. https://doi.org/10.1016/j.geomorph.2018.10.006

Pascual, A., Rodríguez-Lázaro, J., Martínez-García, B., Varela, Z., 2020. Palaeoceanographic and palaeoclimatic changes during the last 37,000 years detected in the SE Bay of Biscay based on benthic foraminifera. Quaternary International 566–567, 323–336. https://doi.org/10.1016/j.quaint.2020.03.043

Poiraud, A., 2012. Les glissements de terrain dans le bassin tertiaire volcanisé du Puy-en-Velay (Massif central, France): caractérisation, facteurs de contrôle et cartographie de l'aléa. Univ. Clermont II.

Poizat, M., 1973. Sédimentation et phénomènes glaciaires et fluvio-glaciaires en Aubrac. Univ. de Provence.

Poizat, M., Rousset, C., 1975. Les calottes de glace quaternaires des Monts d'Aubrac (Massif central, France) : caractéristiques, contexte paléoclimatique. Revue de Géographie Physique et de Géologie Dynamique 17, 171–190.

Ponel, P., Guiter, F., Gandouin, E., Pailles, C., Rioual, P., Djamali, M., Andrieu-Ponel, V., Leydet, M., Van der Putten, N., de Beaulieu, J.-L., 2016. Novel insights from coleopteran and pollen evidence into the Lateglacial/Holocene transition in Aubrac, French Massif Central. Palaeogeography, Palaeoclimatology, Palaeoecology 463, 83–102. https://doi.org/10.1016/j.palaeo.2016.09.020

Ponel, P., Russell Coope, G., 1990. Lateglacial and Early Flandrian Coleoptera from La Taphanel, Massif Central, France: Climatic and Ecological Implications. Journal of Quaternary Science 5, 235–249. https://doi.org/10.1002/jqs.3390050306

Putkonen, J., O'Neal, M., 2006. Degradation of unconsolidated Quaternary landforms in the western North America. Geomorphology 75, 408–419. https://doi.org/10.1016/j.geomorph.2005.07.024

Putkonen, J., Swanson, T., 2003. Accuracy of cosmogenic ages for moraines. Quaternary Research 59, 255–261. https://doi.org/10.1016/S0033-5894(03)00006-1

Rea, B.R., Evans, D.J.A., 2003. Plateau Icefield Landsystems, in: Glacial Landsystems. London.

Rea, B.R., Whalley, W.B., Dixon, T.S., Gordon, J.E., 1999. Plateau icefields as contributing areas to valley glaciers and the potential impact on reconstructed ELAs: a case study from the Lyngen Alps, North Norway. Annals of Glaciology 28, 97–102. https://doi.org/10.3189/172756499781822020

Reille, M., Beaulieu, J.-L. (de), 1988. History of the Würm and Holocene vegetation in western Velay (Massif Central, France): a comparison of pollen analysis from three corings at Lac du Bouchet. Review of Palaeobotany and Palynology 54, 233–248.

Reixach, T., Delmas, M., Braucher, R., Gunnell, Y., Mahé, C., Calvet, M., 2021. Climatic conditions between 19 and 12 ka in the eastern Pyrenees, and wider implications for atmospheric circulation patterns in Europe. Quaternary Science Reviews 260, 106923. https://doi.org/10.1016/j.quascirev.2021.106923

Salgueiro, E., Voelker, A.H.L., de Abreu, L., Abrantes, F., Meggers, H., Wefer, G., 2010. Temperature and productivity changes off the western Iberian margin during the last 150 ky. Quaternary Science Reviews 29, 680–695. https://doi.org/10.1016/j.quascirev.2009.11.013

Samworth, E.A., Warburton, E.K., Engelbertink, G.A.P., 1972. Beta Decay of the ^{26}Al Ground State. Phys. Rev. C 5, 138–142. https://doi.org/10.1103/PhysRevC.5.138

Sanchez Goñi, M.F., Harrison, S.P., 2010. Millennial-scale climate variability and vegetation changes during the Last Glacial: Concepts and terminology. Quaternary Science Reviews 29, 2823–2827. https://doi.org/10.1016/j.quascirev.2009.11.014

Sitzia, L., Bertran, P., Bahain, J.-J., Bateman, M.D., Hernandez, M., Garon, H., de Lafontaine, G., Mercier, N., Leroyer, C., Queffelec, A., Voinchet, P., 2015. The Quaternary coversands of southwest France. Quaternary Science Reviews 124, 84–105. https://doi.org/10.1016/j.quascirev.2015.06.019

Stokes, C.R., Tarasov, L., Blomdin, R., Cronin, T.M., Fisher, T.G., Gyllencreutz, R., Hättestrand, C., Heyman, J., Hindmarsh, R.C.A., Hughes, A.L.C., Jakobsson, M., Kirchner, N., Livingstone, S.J., Margold, M., Murton, J.B., Noormets, R., Peltier, W.R., Peteet, D.M., Piper, D.J.W., Preusser, F., Renssen, H., Roberts, D.H., Roche, D.M., Saint-Ange, F., Stroeven, A.P., Teller, J.T., 2015. On the reconstruction of palaeo-ice sheets: Recent advances and future challenges. Quaternary Science Reviews 125, 15–49. https://doi.org/10.1016/j.quascirev.2015.07.016

Tomkins, M.D., Dortch, J.M., Hughes, P.D., Huck, J.J., Pallàs, R., Rodés, Á., Allard, J.L., Stimson, A.G., Bourlès, D., Rinterknecht, V., Jomelli, V., Rodríguez-Rodríguez, L., Copons, R., Barr, I.D., Darvill, C.M., Bishop, T., 2021. Moraine crest or slope: An analysis of the effects of boulder position on cosmogenic exposure age. Earth and Planetary Science Letters 570, 117092. https://doi.org/10.1016/j.epsl.2021.117092

Valadas, B., 1984. Les hautes terres du Massif central français : contribution à l'étude des morphodynamiques récentes sur versants cristallins et volcaniques. Univ. Panthéon-Sorbonne (Paris I).

Valadas, B., Veyret, Y., 1981. Englacement quaternaire et enneigement actuel de l'Aubrac et du Cantal. Revue géographique des Pyrénées et du Sud-Ouest 52, 201–215. https://doi.org/10.3406/rgpso.1981.4594

Van Vliet-Lanoë, B., Valadas, B., Vergne, V., 1991. La paléogéographie de l'Europe centre-occidentale au Weichsélien. Réflexions sur les paléosols et l'inertie climatique : la place du Massif Central. Quaternaire 2, 134–146. https://doi.org/10.3406/quate.1991.1963

Vergne, V., 1991. Les paysages végétaux d'Artense au Tardiglaciaire et à l'Holocène (Vegetal landscapes in the Artense region during Late-glacial and Holocene). Bulletin de l'Association de Géographes Français 68, 23–28. https://doi.org/10.3406/bagf.1991.1555

Veyret, Y., 1978. Les modelés et formations d'origine glaciaire dans le Massif central français : problèmes de distribution et de limites dans un milieu de moyenne montagne. Univ. Panthéon-Sorbonne (Paris I).

Veyret-Mekdjian, Y., Brousse, P., Delibrias, G., 1978. Première datation d'un épisode glaciaire récent dans le Massif central français. Comptes rendus hebdomadaires des séances de l'Académie des Sciences 286, 1089–1092.

Ward, G.K., Wilson, S.R., 1978. Procedures for comparing and combining radiocarbon age determinations: A critique. Archaeometry 20, 19–31. https://doi.org/10.1111/j.1475-4754.1978.tb00208.x

Wirsig, C., Zasadni, J., Christl, M., Akçar, N., Ivy-Ochs, S., 2016. Dating the onset of LGM ice surface lowering in the High Alps. Quaternary Science Reviews 143, 37–50. https://doi.org/10.1016/j.quascirev.2016.05.001

Zreda, M.G., Phillips, F.M., Elmore, D., 1994. Cosmogenic ^{36}Cl accumulation in unstable landforms: 2. Simulations and measurements on eroding moraines. Water Resources Research 30, 3127–3136. https://doi.org/10.1029/94WR00760